Activity-based probes and chemical proteomics reveal the potential of targeting HMGCS1 for cancer therapy

Sang Ah Yi[1,6], Liang Sun[1,6], Yi Rao[2,3,4], Alban Ordureau[5], Jason S. Lewis[2,3,4], and Heeseon An[1,4*]

[1]Chemical Biology Program, Sloan Kettering Institute, Memorial Sloan Kettering Cancer Center, New York, NY, USA

[2]Department of Radiology, Memorial Sloan Kettering Cancer Center, New York, NY, USA.

[3]Molecular Pharmacology Program, Sloan Kettering Institute, Memorial Sloan Kettering Cancer Center, New York, NY, USA.

[4]Department of Pharmacology, Weill Cornell Graduate School of Medical Sciences, New York, NY, USA

[5]Cell Biology Program, Sloan Kettering Institute, Memorial Sloan Kettering Cancer Center, New York, NY, USA

[6]These authors contributed equally

*Corresponding author: anh@mskcc.org

SUMMARY

HMGCS1 is an underexplored target for inhibitor development compared to other MVP enzymes, despite its unique features, such as a ligandable cysteine. Chemical tools for HMGCS1 are currently limited, with Hymeglusin as the primary inhibitor, although its selectivity has not been fully validated. Here, we report the development of a suite of chemical probes that allow us to evaluate the selectivity, efficacy, and stability of Hymeglusin. Our biological study indicates that Hymeglusin induces proteome changes nearly identical to statins and that concurrently targeting HMGCS1 and HMGCR effectively inhibits the growth of statin-resistant cells and xenograft models without increasing the risk of side effects. Moreover, the proteolysis of HMGCS1 exhibits a more significant anti-proliferative effect than the inhibition. In this context, covalent inhibitors of HMGCS1 can be easily transformed into dual-functional degraders. Collectively, this study provides an extensive toolkit for HMGCS1 and outlines the biological implications of targeting HMGCS1.

KEYWORDS

HMGCS1, Mevalonate, Hymeglusin, HMGCR, statin, chemical proteomics, activity-based probe

INTRODUCTION

Mevalonate is an essential precursor for the biosynthesis of sterols, isoprenoids, vitamin D, and ubiquinone.[1,2] Consequently, the enzymes involved in the mevalonate pathway (MVP) play crucial roles in multiple aspects of cellular physiology, from membrane biology to cell signaling and mitochondrial metabolism.[3] The synthesis of mevalonate begins with the first step, catalyzed by 3-Hydroxy-3-Methylglutaryl-Coenzyme A Synthase 1 (HMGCS1), which condenses acetyl-CoA with acetoacetyl-CoA to produce HMG-CoA. The HMG-CoA then undergoes reduction to mevalonate via HMG-CoA Reductase (HMGCR). Following this, approximately 20 downstream enzymes convert mevalonate into sterols and other non-sterol end-products. Growing evidence indicates that cancer cells exhibit upregulation of MVP enzymes, which may stimulate glucose uptake and various signaling pathways, including RAS, RAB, and RHO.[4-8] This upregulation has also been linked to resistance to various chemotherapies, emphasizing the significance of these enzymes in cancer progression and their ability to manage stress.[9-11] Prior research suggests that inhibiting the mevalonate pathway induces apoptotic death of cancer cells by blocking the geranylgeranylation of proteins.[12,13] Consequently, several enzymes in this pathway, such as HMGCR,

FDPS, GGDPS1, FTase, and GGTase, have been exploited as potential pharmacological targets.[5,7] However, the existing approaches or inhibitors have yet to produce significant clinical anti-cancer activity.[7,14-21]

HMGCS1 represents an underexplored pharmacological target within the mevalonate pathway, despite the fact that it possesses several attractive features that distinguish it from HMGCR and other downstream MVP enzymes. Notably, HMGCS1 contains a catalytic cysteine in its active site that can be readily leveraged for developing covalent inhibitors and chemical probes to enhance potency and sustained efficacy compared to non-covalent inhibitors. Moreover, we previously demonstrated that HMGCS1 levels are directly regulated by the master regulator of cell growth, mTORC1,[22] and an increased requirement for HMGCS1 during the activation of cell proliferation signals makes it a limiting enzyme in cells with hyperactive mTORC1. The extended cellular half-life of HMGCS1, around 10 days, makes it particularly amenable to targeted proteolysis approaches, as the efficacy of induced degradation is enhanced with long-lived proteins.[22] These unique biochemical characteristics of HMGCS1 warrant further exploration into targeting this enzyme with small molecules that can both inhibit its activity and promote its degradation, which may exhibit superior pharmacologic properties compared to existing inhibitors of other enzymes in the mevalonate pathway.

The chemical tools available to perturb the HMGCS1 activity are currently limited, with Hymeglusin serving as the primary small molecule probe.[10,23,24] Identified as an HMGCS1 inhibitor in 1987, Hymeglusin was isolated from Fusarium and Scopulariopsis fungi.[25-30] The co-crystal structure of HMGCS1 and Hymeglusin revealed that Hymeglusin forms a thioester bond with the catalytic cysteine of HMGCS1 following the opening of its lactone ring.[31] A subsequent study showed that this HMGCS1-Hymeglusin adduct is stable *in vitro*, with an estimated half-life of 55 hours.[26] The same study also showed that Hymeglusin-mediated inhibition of HMGCS1 in cells is reversed within 30 minutes after withdrawal when measured by the conversion of radioactive acetate into cholesterol.[26] However, the occupancy level of the intracellular HMGCS1 catalytic cysteine and the cause of this increased reversibility of Hymeglusin remains unclear, primarily due to the lack of tools that allow direct monitoring. Additionally, a comprehensive quantitative analysis of the reactivity of Hymeglusin toward the global proteome, as well as its effects on reshaping the proteome landscape, has not been reported.

In the present study, we have developed activity-based probes for HMGCS1, functionalized with fluorescent dye or biotin handles, that facilitate the investigation of the effects of covalent inhibition of HMGCS1 in human cells. By combining these probes with proteomics analyses, we show that Hymeglusin specifically reacts with the catalytic cysteine of HMGCS1 in cells. Hymeglusin treatment induces global proteomic changes that are nearly identical to those induced by the HMGCR inhibitor, Simvastatin. Our unbiased data support the selective inhibition of mevalonate synthesis by Hymeglusin and reveal non-redundant functions of HMGCS1 and HMGCR outside the mevalonate pathway. Consequently, the concurrent targeting of both enzymes potentiates inhibition of mevalonate synthesis, leading to increased anti-cancer effects in cells and in mouse xenograft models. We also show that targeted proteolysis of HMGCS1 exhibits a more potent anti-proliferation effect than inhibition and that HMGCS1 covalent inhibitors can be transformed into bifunctional degraders that serve as both inhibitors and degraders. In conclusion, this study presents a comprehensive toolkit for inhibiting and analyzing HMGCS1 activity and provides cell biological and pharmacological effects of this intervention.

RESULTS

Hymeglusin-fluorescence conjugates monitor occupancy of the HMGCS1 active site.

HMGCS1 is a 57 kDa protein known to form tight homodimers in cells and *in vitro*.[22,32] A previous co-crystal structure showed that Hymeglusin forms a covalent bond with the catalytic cysteine of HMGCS1, thereby inhibiting its enzymatic activity (**Fig. 1A**).[33] While Hymeglusin has been used as a representative inhibitor of HMGCS1 for biological studies,[10,23,24] its proteome-wide selectivity has not been evaluated quantitatively. This lack of comprehensive evaluation creates uncertainties about its biological implications and on-target effects. We, therefore, synthesized fluorescent probes by conjugating the Hymeglusin warhead to two different dyes, fluorescein or tetramethylrhodamine (TMR), through a linker (**Fig. 1B**). The Hymeglusin-fluorecein (HG-FL) probe was then incubated with either wild-type (WT) or a catalytically inactive HMGCS1

harboring a Cys-Ala substitution *in vitro*, after purifying them from HEK293T cells (**Fig. 1C**). In-gel fluorescence analysis showed a signal exclusively in wild-type HMGCS1, indicating that HG-FL binds the catalytic cysteine residue. When recombinant HMGCS1 was pre-treated in vitro with different concentrations of Hymeglusin before adding HG-FL, the fluorescent signal decreased in a dose-dependent manner (**Fig. 1D**). HG-FL binding to HMGCS1 was disrupted in the presence of a reducing agent, dithiothreitol (DTT), which may cleave the thioester bond formed between Cys129 and Hymeglusin. However, the strong resistance of this interaction under denaturing conditions implied a tight binding of Hymeglusin to the hydrophobic pocket, which hinders the access of DTT for trans thiolation reaction (**Fig. 1E**). We subsequently investigated whether HG-fluorescence probes could be used to monitor the occupancy of the catalytic cysteine residue within intracellular HMGCS1 (**Fig. 1F,** upper panel). WT HEK293T cells were treated with Hymeglusin for 2 hours, followed by cell lysis, and incubation with HG-FL. Subsequent in-gel fluorescence analyses revealed a fluorescence band that was reversed upon pre-incubation of cells with Hymeglusin (**Fig. 1F**, bottom left panel). CRISPR-engineered HCT116 cells expressing endogenous HMGCS1-FKBP12^{F36V} or HMGCS1-mEGFP fusion protein showed similar results when probed by either HG-FL or HG-TMR, with the shifts in molecular weight that match with HMGCS1 chimera (**Fig. 1F**, bottom middle/right panels). The same gels were then subjected to immunoblotting for HMGCS1 detection, and the fluorescent bands coincided with the bands detected by the anti-HMGCS1 antibody. These data indicate that HG-fluorescence probes can serve as activity-based probes for HMGCS1.

Does Hymeglusin occupancy of the HMGCS1 catalytic cysteine lead to the depletion of cellular HMG-CoA, the product of HMGCS1 enzymatic activity? Previous investigations have demonstrated that the accumulation of HMG-CoA in cells, resulting from the inhibition of HMGCR by statins, facilitates a non-enzymatic reaction with fatty acid synthase (FASN), leading to the formation of HMG-modified FASN (**Fig. 1G,** upper panel).[34] The presence of this modification can be effectively monitored using an HMG-specific antibody.[35] Notably, the overall reactivity of this antibody has been found to correlate with intracellular levels of HMG-CoA. Indeed, when HCT116 cells expressing endogenous HMGCS1-FKBP12^{F36V} fusion protein were treated with Simvastatin, an HMG positive band appeared around 240 kDa range (**Fig. 1G**, bottom panel, first two lanes). The addition of the dTAGv1 ligand, which recruits the VHL-containing E3 ligase complex to the FKBP12^{F36V} tag and induces the degradation of HMGCS1-FKBP12^{F36V}chimera, caused the disappearance of the HMGylated protein signal (**Fig. 1G,** bottom panel, third lane, and **Fig. S1A**).[22,36] This indicates that the cellular HMG-CoA level dropped in the absence of HMGCS1. Treatment with increasing concentrations of Hymeglusin similarly led to a progressive decrease in the HMGylated protein intensity, indicating inhibition of HMGCS1 activity. Of note, statin treatment induced a substantial increase in HMGCS1 and HMGCR levels due to feedback effect mediated by the SREBP2 transcription factor.[37]

Hymeglusin reacts highly selectively with HMGCS1 in human cells.

We next evaluated the reactivity of Hymeglusin toward the human proteome using an unbiased chemical proteomics approach. To conclusively identify the Hymeglusin-labeled proteins using mass spectrometry, we synthesized the Hymeglusin-biotin (HG-Biotin) probe (**Fig. 2A**, top). HEK293T cells were either treated with Hymeglusin or DMSO for 30 min prior to incubation with HG-biotin. The proteins labeled with HG-biotin were enriched using streptavidin beads, and the eluates were analyzed using a 6-plex tandem-mass-tag (TMT)-based quantification. Our proteomic analysis revealed that HMGCS1 is the only significantly enriched protein that was displaced by the pretreatment with Hymeglusin (12-fold increase, 50 peptides detected), demonstrating Hymeglusin's high selectivity for HMGCS1 (**Fig. 2B**). An orthogonal immunoblotting assay confirmed the strong enrichment of HMGCS1 by HG-biotin (**Fig. 2C**). In contrast, endogenously biotinylated proteins such as ACACA (18 peptides), PCCA (19 peptides), and MCCC1 (14 peptides), were enriched regardless of Hymeglusin pre-treatment, as a consequence of their interaction with streptavidin (**Table S1**). Consistently, the HG-FL assay on HEK293T cells that were pretreated with increasing concentrations of Hymeglusin revealed a single strong fluorescence signal around 57 kDa, corresponding to the molecular weight of HMGCS1 (**Fig. 2D**). This signal disappeared when the cells were pretreated with 250-500 nM Hymeglusin. We conclude that Hymeglusin is a potent and selective inhibitor of HMGCS1, making it a suitable tool for examining the downstream biological effects of acute HMGCS1 inhibition.

149
150 **The inhibition or degradation of HMGCS1, or inhibition of HMGCR, results in identical changes to**
151 **the proteome.**
152 To gain a deeper understanding of the cellular response to the inhibition of HMGCS1, we analyzed global
153 proteomic changes following Hymeglusin treatment (**Fig. 3A**, left). We compared the proteome alterations
154 caused by the acute degradation of HMGCS1 by using the HCT116 HMGCS1-FKBP12^{F36V} knock-in cells,
155 which may decouple any side effects of Hymeglusin and non-enzymatic roles of HMGCS1 if they exist. We
156 also compared the proteome changes induced by the inhibition of HMGCR, as HMGCS1 and HMGCR are
157 the first two enzymes in the mevalonate pathway (**Table S2**). If these two enzymes have additional functions
158 outside the mevalonate pathway, it may be evident in the proteome changes. Immunoblotting analysis
159 showed that dTAGv1 treatment for 24 hours led to the expected depletion of HMGCS1 and the upregulation
160 of unprenylated RhoA and HMGCR, a known feedback effect (**Fig. 3A**, right).[38] Hymeglusin treatment also
161 resulted in an increase of RhoA and HMGCR, along with HMGCS1. Similarly, statin treatment caused a
162 significant increase in RhoA, HMGCR, and the emergence of HMGylated FASN. These data suggest that
163 each condition results in a comparable degree of mevalonate flux perturbation. Accordingly, the TMT-based
164 proteomics approach was applied to the cells under the corresponding conditions in four replicates, and the
165 overall quality of the samples was assessed again through immunoblotting (**Fig. 3B,C**). The following mass-
166 spectrometry analysis revealed the relative abundance of 9,881 proteins across all 16 samples without
167 missing values. Principal component analysis showed that replicates of each sample clustered together,
168 indicating consistency among the replicates (**Fig. S2A**). Notably, only the untreated cells showed a distinct
169 separation, while the cells treated with the mevalonate pathway inhibition formed a closely clustered group.
170 For example, proteome profiles from cells treated with Simvastatin and Hymeglusin showed nearly identical
171 results, indicated by a strong Pearson correlation coefficient of 0.97 (**Fig. S2B**). A similarly high correlation
172 coefficient (Pearson r = 0.95) was observed when comparing Hymeglusin-treated cells with those subjected
173 to HMGCS1 degradation (**Fig. S2C**). These unbiased proteomics data reveal that 1) Hymeglusin produces
174 proteome changes that are highly specific to HMGCS1 inhibition, 2) HMGCS1 depletion causes proteome
175 changes driven by the loss of its enzymatic function, and 3) targeting HMGCS1 and HMGCR leads to the
176 nearly identical proteomic changes, reinforcing their essential role in the mevalonate pathway.
177
178 12% of the total proteome (1,200 of 9,881 proteins) showed significant changes within 24 hours of
179 Hymeglusin treatment. It was evident that the inhibition of the mevalonate pathway substantially stimulated
180 the production of a subset of the proteome, with 168 proteins increasing by more than two-fold while 24
181 proteins decreased (**Fig. 3D**). Gene Ontology (GO) analysis of the significantly upregulated proteins (> 2-
182 fold, 168 proteins) for their cellular compartment indicated that the proteins in the secretory pathway are
183 significantly enriched (**Fig. 3E**). Functionally, proteins involved in regulating cell migration and signaling
184 receptor binding were prominent (30 and 38 proteins, respectively), aligning with the role of the mevalonate
185 pathway in regulating small GTPase family members, such as Rho, Rab, and Ras. A notable increase was
186 also observed in ~ 20 enzymes within the mevalonate pathway across the various treatment conditions
187 (**Fig. 3F**). All three inhibitory conditions resulted in a similar induction of the mevalonate pathway enzymes.
188 These findings are consistent with prior reports of a transcriptional feedback mechanism mediated by Sterol
189 Regulatory Element-Binding Protein 2, which is triggered upon the inhibition of MVP enzymes.[39]
190 Significantly downregulated proteins (greater than 2-fold difference, 24 proteins) included seven proteins
191 involved in the mitotic spindle checkpoint, indicating that cell cycle arrest was initiated, likely as a sign of
192 early-stage apoptosis (**Fig. 3D**). In this context, BCL2L12, an anti-apoptotic regulator, was downregulated
193 by more than 2-fold. Mevalonate is a precursor for not only sterols but also isoprenoids that are essential
194 for post-translational modifications, such as farnesylation and geranylgeranylation. Three proteins targeted
195 by farnesylation (RAB20, RAB29, RAB12) and two proteins for geranylgeranylation with a CAAX motif
196 (MIEN1 and FBXO10) were significantly downregulated, suggesting their destabilization due to the loss of
197 prenylation. When we examined the changes in prenylation substrates on a broader scale, we found many
198 of them among the statistically significant hits. Intriguingly, they showed divergent expression changes upon
199 the inhibition of mevalonate production (**Fig. 3G**). Their downregulation may stem from instability caused
200 by the lack of prenylation in the newly produced proteins, while the up-regulated proteins may be a result

201 of their transcriptional feedback effect mediated by SREBP2, producing unprenylated RHO and RAB
202 proteins. In any case, their cellular functions may be negatively affected by the loss of prenylation. In
203 summary, the inhibition or degradation of HMGCS1, or the inhibition of HMGCR by statins, results in a
204 similar alteration of the global proteome that is characterized by the induction of the MVP enzymes and the
205 substrates of the downstream metabolites, isoprenoids.
206
207 **Simultaneous targeting HMGCS1 and HMGCR produces a synergistic anti-cancer response**.
208 Repurposing statins has attracted significant interest as a strategy for treating cancer.[20] However, many
209 patients were non-responsive to statin treatment. Prior studies have suggested that cells demonstrating
210 feedback upregulation of the MVP enzymes, particularly HMGCS1, tend to exhibit strong statin
211 resistance.[40-42] We tested this by using seven cell lines with different lineages. Simvastatin treatment for 24
212 hours led to varying levels of HMGCS1 induction (**Fig. S3A, B**). Among the seven cell lines, HCT116
213 showed a 2.5-fold increase in HMGCS1, while the HMGCS1 levels in HEK293T or MFE296 cell lines
214 remained unaltered (**Fig. S3C**). The following cell viability assay on HCT116 and HEK293T cells indicated
215 that HCT116 cells are highly resistant to Simvastatin treatment, while HEK293T cells were relatively more
216 sensitive (**Fig. S3D**). Colony formation assays on HCT116 and MFE296 cells also showed resistance for
217 HCT116, whereas MFE296 cells exhibited a more sensitive response (**Fig. S3E**). Based on our data and
218 the prior study, we conclude that the increased production of HMGCS1 upon statin treatment may contribute
219 to the low efficacy of statins in HCT116.
220
221 The strong correlation observed between changes in the global proteome caused by the inhibition of
222 HMGCS1 and HMGCR suggests that simultaneously targeting both enzymes may more effectively inhibit
223 the mevalonate metabolic pathway. This could address the current limitation of statin efficacy in anti-cancer
224 therapy, especially in cells that are resistant to statins. We, therefore, examined if simultaneous targeting
225 of HMGCS1 and HMGCR would enhance the anti-proliferative effect of the monotherapy using HCT116
226 cells (**Fig. 4A**). In a colony formation assay, treatment with a statin alone resulted in a ~30% decrease in
227 the number of colonies, while Hymeglusin alone had a negligible effect. In contrast, combined treatment
228 with Symvastatin and Hymeglusin resulted in significant inhibition of colony formation. Similarly, we
229 examined the effect of HMGCS1 degradation on cell proliferation, both individually and in combination with
230 a statin, using HCT116 cells expressing endogenous HMGCS1-FKBP12^{F36V} fusion protein (**Fig. 4B**). In
231 these cells, Simvastatin treatment resulted in a substantial increase in endogenous HMGCS1-FKBP12^{F36V},
232 as expected, whereas addition of dTAGv1 nearly depleted HMGCS1 via induced degradation. Treatment
233 of dTAGv1 in these cells led to a 60% reduction in colony numbers, while co-treatment with dTAGv1 and
234 Simvastatin resulted in nearly complete inhibition of colony formation (**Fig. 4C,D)**. Similarly, cell viability
235 assay results gained from the monolayered cell culture system indicated that the addition of dTAGv1 ligand
236 significantly enhanced the IC_{50} of Simvastatin, decreasing from 15.6 μM to 1.3 μM (**Fig. 4E**). As a control,
237 we treated wild-type HCT116 cells with the dTAGv1 ligand, which exhibited no change in the IC_{50} of
238 Simvastatin, confirming that the observed change in IC_{50} was due to the degradation of HMGCS1 (**Fig. 4E,**
239 bottom). Importantly, the cell death caused by the joint treatment was rescued by supplementing the media
240 with geranylgeranyl alcohol (GGOH), a precursor of the downstream metabolite of the mevalonate,
241 indicating that the enhanced cytotoxicity arises from the impairment of the mevalonate synthesis (**Fig. 4F**).
242
243 Lastly, we performed the equivalent study using the mouse xenograft model after implanting HCT116
244 HMGCS1-FKBP12^{F36V} cells (**Fig. 4G,H**). Four groups of mice were subjected to two treatment regimens
245 over a two-week interval, including saline control, oral Simvastatin three times a week, weekly i.p. injection
246 of dTAGv1, and the combination of Simvastatin and dTAGv1. The group of mice that received both
247 Simvastatin and dTAGv1 exhibited a synergistic effect on tumor growth suppression that lasted for 40 days.
248 In contrast, administration of Simvastatin or dTAGv1 ligand injection alone did not show a significant
249 difference compared to the PBS-treated control group. Overall data suggest that dual targeting of HMGCS1
250 and HMGCR may offer potential benefits, and the targeted proteolysis approach for HMGCS1 perturbation
251 could demonstrate greater efficacy compared to inhibition.
252
253 **Novel bifunctional molecules both inhibit and degrade HMGCS1.**
254 The superior cytotoxicity of HMGCS1 proteolysis prompted us to test whether we could design small
255 molecule ligands that both inhibit and induce degradation of HMGCS1 to achieve longer-lasting effects and

higher efficacy compared to inhibition alone. We previously reported that the half-life of the HMGCS1 protein spans several days in cells with active mTORC1, the master regulator of cell growth.[22] Thus, HMGCS1 is a particularly amenable target for this targeted proteolysis approach for rapidly dividing cancer cells with active mTOR. We, therefore, investigated whether we could convert the HMGCS1 inhibitor into a bifunctional molecule by conjugating Hymeglusin to a ligand that recruits either Cereblon (CRBN) or von Hippel-Lindau (VHL) E3 ligase complex (**Fig. 5A**). Since the linkers are crucial to degradation efficacy, we tested linear linkers of varying lengths, from a short C4 hydrocarbon chain (proteolysis-targeting chimera1 or PROTAC1) to a linker containing 6-polyethyleneglycols (PEG) (PROTAC 5). Comparative degradation analysis of the five HG-PROTAC molecules in HEK293T, RPE1, and HeLa cells consistently showed that HG-PROTAC4, which recruits the VHL E3 complex and contains three PEG in the linker, induces the most pronounced reduction of HMGCS1, in the presence of translation inhibitor cycloheximide (**Fig. 5B**). The reduction observed with HG-PROTAC4 treatment was dependent on the ubiquitin-activating E1 enzyme, confirming that the ubiquitination-dependent degradation of HMGCS1 was the cause of reduction (**Fig. 5C**). In-gel fluorescence analysis of HG-PROTAC4 treated cells using HG-FL showed that HG-PROTAC4 enters cells within 15 minutes, despite its relatively large molecular weight of 924 Da, and that it fully occupies the catalytic cysteine of HMGCS1 (**Fig. 5D**). Following immunoblotting assay revealed that HMGCS1 degradation occurs at a slower rate, with a 50% reduction in protein levels observed after 8 hours. These data indicate that HG-PROTAC4 initially functions as an inhibitor, as early as 15 min, and subsequently as a degrader in situ. Our findings establish a rationale for the development of more efficacious bifunctional degraders that target the HMGCS1 catalytic cysteine. Nonetheless, HG-PROTAC4 exhibited limited efficacy in diminishing cell proliferation within HCT116 cells. Similarly, the parental molecule, Hymeglusin, did not elicit any cytotoxic effects in either HCT116 or HEK293T cells (**Fig. S4A**). This observation prompted us to further investigate the long-term stability of Hymeglusin and its derivatives.

Hymeglusin warhead exhibits poor serum stability.

Prior investigations using murine models administered with Hymeglusin reported an 80% reduction in cholesterol synthesis within 30 min and a complete loss of inhibitory function by 180 min when measured by the conversion of ^{14}C-labeled acetate into plasma cholesterol. It was speculated that this effect may be due to the reversible nature of the thioester bond formed between Hymeglusin and HMGCS1. However, the precise kinetics underlying the decline in Hymeglusin efficacy and the mechanism behind its loss of efficacy remain to be determined. Considering that researchers have utilized Hymeglusin as an inhibitor of HMGCS1 in a range of cell culture models, elucidating this limitation could be crucial for its appropriate application. Our use of the HMGCS1 activity-based probes enabled us to monitor the occupancy of the catalytic cysteine in HMGCS1 by Hymeglusin over time. After 8 hours of treatment with 0.5 μM Hymeglusin, we observed the emergence of the catalytically active HMGCS1 that was labeled with HG-FL, a trend that became more pronounced after 16 hours in HEK293T, HCT116, or HepG2 cells (**Fig. 6A,B**). HG-PROTAC4 showed a similar rebound of the probe-unoccupied HMGCS1 at the 8h time point (**Fig. 6C**). These data indicate that HMGCS1 labeling is not maintained over the long term, which aligns with the absence of sustained efficacy in the antiproliferative effects observed with Hymeglusin or HG-PROTAC4 treatment. Interestingly, the removal of serum from the culture media led to a delayed restoration of active HMGCS1 levels, indicating that serum plays a role in the short-term efficacy of Hymeglusin (**Fig. 6D**). Indeed when Hymeglusin was pre-incubated in DMEM with 10% FBS for 16 hours before being added to the cells, the catalytic cysteine of HMGCS1 was not effectively inhibited anymore (**Fig. 6E,F**). In contrast, pre-incubation in DMEM without 10% FBS did not reduce the efficacy of Hymeglusin. Additionally, we observed intense labeling of bovine serum albumin (BSA) by HG-FL after incubating them for one hour *in vitro* (**Fig. 6G**). The labeling persisted even after boiling for 5 minutes in denaturing conditions, suggesting a strong interaction between HG-FL and BSA. Thus, poor serum stability may restrict the long-term use of Hymeglusin or its derivatives in cell and *in vivo* studies, as human serum typically contains ~ 40 mg/ml of albumin.

DISCUSSION

The mevalonate pathway is a well-established focus of interest for chemists and biologists, given its critical role in cholesterol biogenesis and prenylation. Prenylation, in particular, is essential for the proper function of several oncogenic proteins, such as RAS, which underscores its contribution to cancer progression. Consequently, several enzymes in the mevalonate pathway have received substantial attention in

310 pharmaceutical research for inhibitor development. However, the initial enzyme of the pathway, HMGCS1,
311 has received relatively little focus, overshadowed by HMGCR and the established use of statins. We have
312 recently discovered that HMGCS1 functions as a gatekeeper of this pathway, especially in cells with
313 hyperactive mTORC1 signaling.[22] HMGCS1 senses and responds to fluctuations in mTORC1 activity,
314 paralleling the critical role of HMGCR in sensing and responding to changes in membrane sterol levels.
315 Moreover, the presence of a ligandable cysteine in HMGCS1 makes it a particularly unique and
316 advantageous target for probe development, which can significantly facilitate investigations into both the
317 mechanisms of inhibitor action and potential resistance.

318 Currently, few tools are available to interrogate HMGCS1. Among them, Hymeglusin, a natural product
319 derived from fungi, stands out as the primary tool utilized in the field since its discovery in the 1980s.[25-29,43]
320 Despite its widespread use, the selectivity and overall efficacy of Hymeglusin in cells have not been
321 thoroughly evaluated since the 1990s, raising concerns about its suitability as a tool compound. This
322 prompted us to assess its cellular potency and selectivity by developing activity-based probes inspired by
323 the Hymeglusin warhead and leveraging modern technologies, such as proteomics. Our unbiased
324 analyses, grounded in chemical biology approaches, revealed that Hymeglusin is a potent and highly
325 selective inhibitor of HMGCS1 in HEK293T cells, with a concentration of 0.5 μM fully saturating the catalytic
326 cysteine of HMGCS1 in cells. However, we also determined that Hymeglusin has extremely poor serum
327 stability, which serves as a cautionary note for the field when using it as a research tool. Nevertheless, our
328 comprehensive data led us to consider Hymeglusin a viable tool for studying the short-term pharmacologic
329 effects of HMGCS1 inhibition, provided we carefully monitor its intracellular stability and activity with our
330 activity-based probes.

331 After carefully characterizing Hymeglusin, we explored the effect of inhibiting HMGCS1 using Hymeglusin
332 and an additional method that incorporates a chemical genomic approach to induce the degradation of
333 HMGCS1. Proteomic analysis of cells following HMGCS1 inhibition or degradation, or HMGCR inhibition,
334 revealed surprisingly similar proteome changes in 24 hours. This result indicates that targeting both
335 enzymes simultaneously may enhance drug efficacy without amplifying the risk of potential side effects
336 from either inhibitor. Our follow-up cell biological and xenograft studies support this notion that dual
337 targeting of HMGCS1 and HMGCR potentiates the anti-cancer effect of statin monotherapy.

338 Comparative analysis of HMGCS1 inhibition by Hymeglusin or of HMGCS1 degradation using the
339 chemically induced tag system (dTAG) demonstrated the superior potency of the degradation approach in
340 inhibiting cancer cell proliferation. These results suggest that the hybrid molecule, which could inhibit and
341 also induce degradation of HMGCS1, may confer a better efficacy than the inhibitor. Bifunctional molecules
342 have potential therapeutic advantages over the monofunctional inhibitor.[44,45] In the case of HMGCS1, the
343 bifunctional molecule can counteract the compensatory upregulation of HMGCS1 through its degradation.
344 As the half-life of the HMGCS1 protein spans several days, the drug-induced degradation of HMGCS1 can
345 be prolonged longer than the inhibitors. Additionally, covalent PROTACs have been shown to enhance
346 cellular uptake and target selectivity.[46] We thus synthesized bisubstrate inhibitor candidates of HMGCS1 to
347 test their therapeutic potential. Notably, the increased molecular weight of the bisubstrate ligand molecules,
348 HG-PROTACs, did not compromise cell penetration or their inhibitory function, as assessed by our
349 fluorescence probe that measures the occupancy of the catalytic cysteine. Moreover, induction of HMGCS1
350 degradation was observed following inhibition, highlighting their role as dual-functional molecules. Overall,
351 our findings highlight the potential of targeting HMGCS1 either as a monotherapy or in combination with
352 statins, emphasizing the benefits of the induced proteolysis approach in this context.

353 In summary, this study reports new chemical biology tools for an important yet underexplored metabolic
354 enzyme within cells, HMGCS1. It offers insights into how targeting HMGCS1—either alone or together with
355 HMGCR—can lead to alterations in the identical cellular proteome while potentiating their anti-proliferation
356 effect. Furthermore, the study holds potential for developing drug-like inhibitors or bisubstrate degraders of
357 HMGCS1 by utilizing the activity-based probes developed in this study.

358 ***Limitations of the study***

Further investigation is needed to determine how serum influences the instability of Hymeglusin. One possibility is that a cysteine at amino acid position 34, which does not form disulfide bonds like the other 34 cysteines, may interact with the lactone moiety of Hymeglusin.[47] Another possibility is that the structure of Hymeglusin resembles that of fatty acids. Albumin has well-characterized fatty acid binding pockets, with at least seven known pockets that could potentially interact with Hymeglusin.[48] A second limitation of the present study is the short-term efficacy of HG-PROTAC molecules on HMGCS1 degradation, which may reflect the instability of the Hymeglusin warhead. Additionally, many covalent PROTACs, including our Hymeglusin-based PROTACs, cannot be recycled once they engage the target cysteine, thus contributing to the observed reduction in intracellular potency. This reinforces the need to develop small molecule probes for HMGCS1 with optimized stability. In this context, our Hymeglusin-fluorescence probes will serve as useful tools for activity-based screening of such molecules in vitro and in cells. Lastly, the mitochondrial HMG-CoA synthase, HMGCS2, shares approximately 60% sequence identity with HMGCS1, which may be a target of Hymeglusin. HMGCS2 exhibits tissue-specific expression profiles, unlike the universal expression of HMGCS1. Therefore, this aspect should be considered when using Hymeglusin for cell lines that express HMGCS2.

RESOURCE AVAILABILITY

Lead contact

Further information and requests for resources and reagents should be directed to and will be fulfilled by lead contact Heeseon An, anh@mskcc.org

Materials availability

This study did not produce new materials.

Data and code availability

- All unique identifiers, and web links for publicly available datasets are presented within the main text or the supplementary materials. The proteomic data generated in this paper will be deposited to the MassIVE repository with the dataset identifier:
- This paper does not report any original code.
- Any additional information required to reanalyze the data reported in this paper is available from the lead contact upon request.

ACKNOWLEDGMENTS

We thank Brittany Pham for helping with the cell viability assay. We thank Beth Moorefield, Ph. D., for providing critical feedback and review of the manuscript. This work was supported by MSKCC Josie Robertson Foundation. This research was also supported by NIH R35 CA232130 (J.S. L) and partly by the Memorial Sloan Kettering Cancer Center Support Grant P30CA008748 (A.O., J.S.L., and H.A.)

AUTHOR CONTRIBUTIONS

Conceptualization, S.A.Y., L.S. and H.A.; methodology, S.A.Y., L.S., Y.R., and A.O.; Investigation, S.A.Y., L.S., Y.R., and A.O.; writing—original draft, S.A.Y., L.S., and H.A.; writing—review & editing, Y.R., A.O. and J.L.; funding acquisition, A.O., J.L., and H.A.; supervision, H.A.

DECLARATION OF INTERESTS

The authors declare no competing interests.

Figure 1

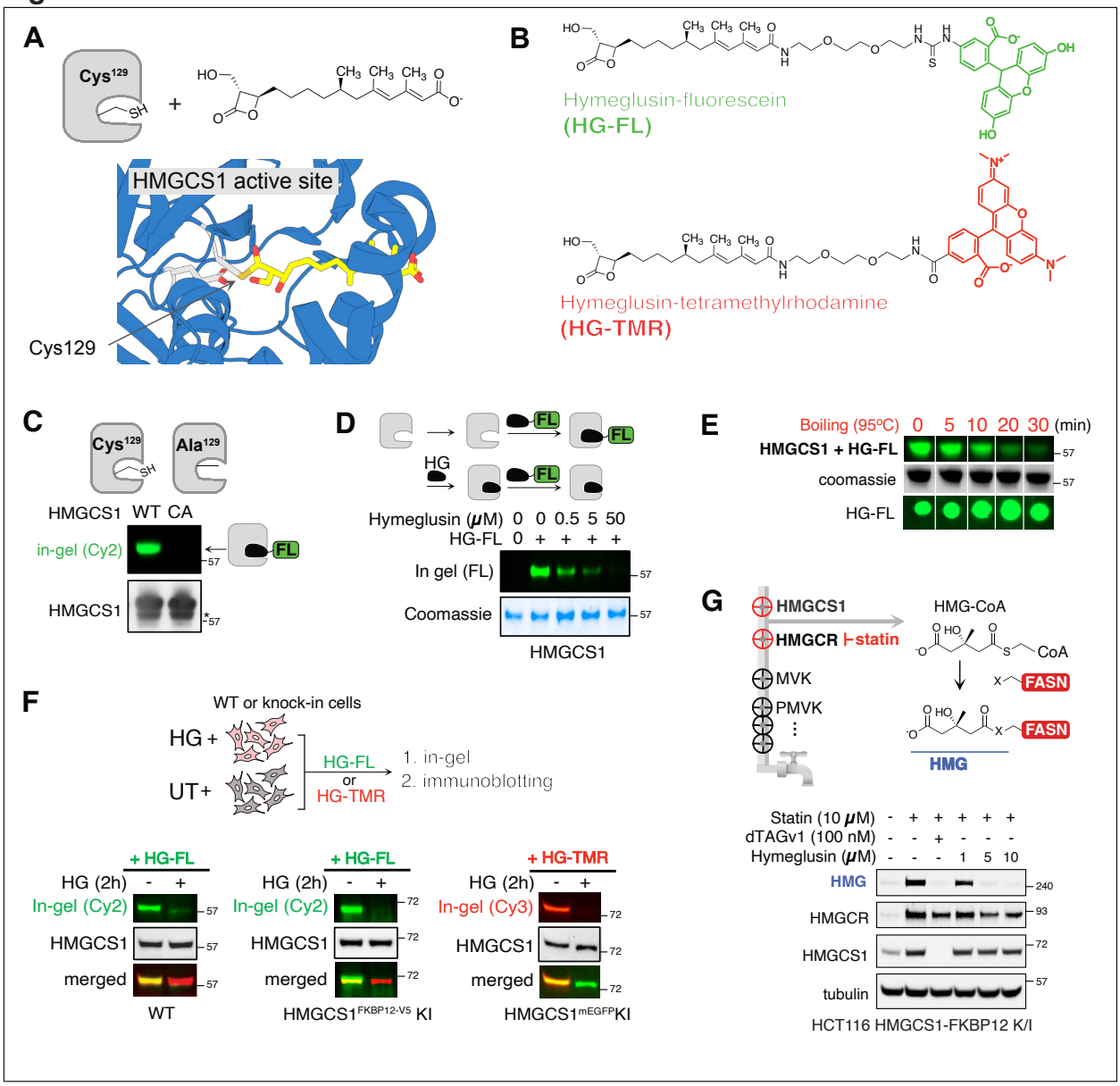
A
Cys129
SH
HMGCS1 active site
Cys129
B
Hymeglusin-fluorescein
(HG-FL)
Hymeglusin-tetramethylrhodamine
(HG-TMR)
C
Cys129
Ala129
HMGCS1 WT CA
in-gel (Cy2)
FL
HMGCS1
D
FL
HG
Hymeglusin (μM) 0 0 0.5 5 50
HG-FL 0 + + + +
In gel (FL)
Coomassie
HMGCS1
E
Boiling (95ºC) 0 5 10 20 30 (min)
HMGCS1 + HG-FL
coomassie
HG-FL
G
HMGCS1
HMGCR
statin
MVK
PMVK
HMG-CoA
CoA
FASN
HMG
Statin (10 μM) - + + + + +
dTAGv1 (100 nM) - - + - - -
Hymeglusin (μM) - - - 1 5 10
HMG
HMGCR
HMGCS1
tubulin
HCT116 HMGCS1-FKBP12 K/I
F
WT or knock-in cells
HG +
UT+
HG-FL
or
HG-TMR
1. in-gel
2. immunoblotting
+ HG-FL
HG (2h) - +
In-gel (Cy2)
HMGCS1
merged
WT
+ HG-FL
HG (2h) - +
In-gel (Cy2)
HMGCS1
merged
HMGCS1FKBP12-V5 KI
+ HG-TMR
HG (2h) - +
In-gel (Cy3)
HMGCS1
merged
HMGCS1mEGFPKI

FIGURE 1. Hymeglusin-fluorescence conjugates serve as activity-based probes for HMGCS1.

(A) A schematic of the HMGCS1 and Hymeglusin (top) and the zoomed-in co-crystal structure of the Hymeglusin-bound HMGCS1 (bottom, PDB: 2F9A)

(B) Chemical structures of the Hymeglusin-fluorescein (HG-FL) and Hymeglusin-tetramethylrhodamine probes (HG-TMR).

(C) Comparative in-gel fluorescence assay of wild-type (WT) or a catalytically inactive HMGCS1 mutant (C129A, CA) confirms the labeling of the catalytic cysteine of HMGCS1 with HG-FL.

(D) Top: scheme of the HG-FL competition reaction *in vitro*. Bottom: incubating recombinant HMGCS1 (1 μg) with increasing concentrations of Hymeglusin for 30 minutes results in a decrease of HG-FL labeled HMGCS1.

(E) The labeling of HMGCS1 by HG-FL was reversed after boiling at 95°C for at least 20 minutes in a buffer containing 2% LDS and 50 mM DTT. SDS-PAGE resolved HMGCS1 before the in-gel fluorescence analysis, while the stability of the HG-FL probe in the given conditions was assessed by dot blot in parallel.

(F) HEK293T WT and HCT116 knock-in (KI) (HMGCS1-FKBP12^{F36V} or HMGCS1-mEGFP) cells were treated with Hymeglusin (4 μM for WT, 0.5 μM for KI, 2 hours) or left untreated, followed by cell lysis and incubation with HG-FL or HG-TMR for one hour. After in-gel fluorescence analysis, the gels were transferred to the PVDF membrane for immunoblotting using an anti-HMGCS1 antibody.

(G) HMGCR inhibition by statins leads to the accumulation of HMG-CoA in cells. This results in the non-enzymatic modification of several residues in the FASN active site by the HMG moiety, which can be detected by the anti-HMG antibody (top). HCT116 cells expressing endogenous HMGCS1-FKBP12^{F36V} were treated with the indicated chemicals for 24 hours, followed by immunoblotting analysis using anti-HMG, anti-HMGCR, anti-HMGCS1, and anti-tubulin antibodies (bottom).

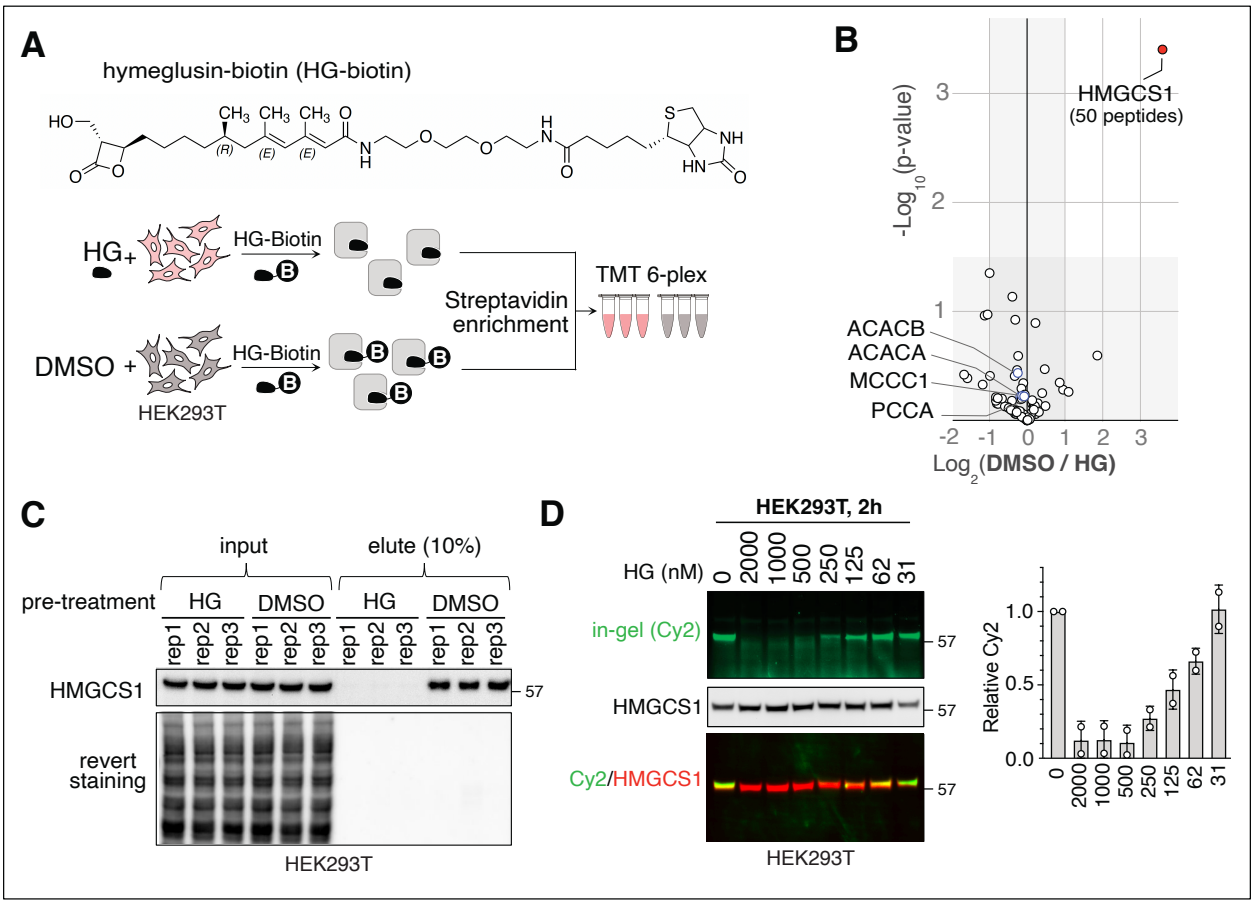

FIGURE 2. Hymeglusin is a highly selective inhibitor of HMGCS1 in human cells.

(A) The structure of the Hymeglusin-biotin probe is shown at the top, and the workflow of competitive affinity purification mass-spectrometry (AP-MS) using Hymeglusin-biotin combined with TMT-6 plex methods is shown at the bottom.

(B) HEK293T cells were either treated with HG (1 μM, 30 min) or DMSO, followed by further incubation with the in-house HG-biotin probe (1 μM, 2 h). After streptavidin beads enrichment, the eluates were analyzed through tandem-mass-tag-based proteomic analysis. The proteomic data is presented as a volcano plot of the $-\log_{10}$-transformed p-value versus the $\log_2$-transformed ratio of DMSO/Hymeglusin pre-treated cells. n = 3 biological replicates. p-values were calculated by two-sided Welch's t-test (adjusted to 1% FDR for multiple comparisons).

(C) HEK293T cells were treated as described in panel A. After streptavidin enrichment, the eluates were subjected to immunoblotting using the anti-HMGCS1 antibody. Rep: replicate.

(D) HEK293T cells were treated with increasing concentrations of Hymeglusin for 2 hours, followed by HG-FL treatment and in-gel fluorescence analysis. The same extracts were then transferred to a PVDF membrane to probe for HMGCS1 using immunoblotting. The average of two replicates is shown on the right.

Figure 3

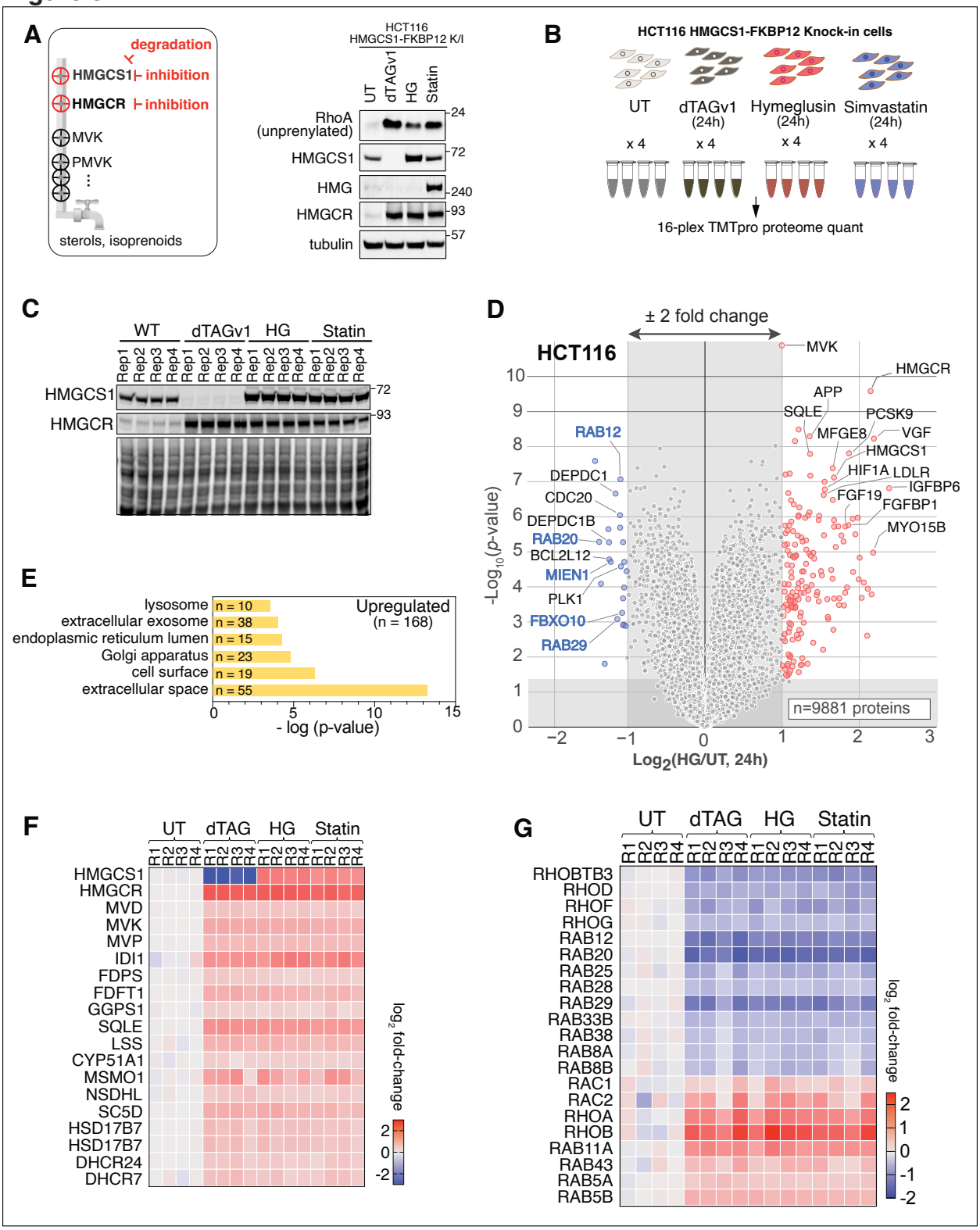
A
degradation
HMGCS1
inhibition
HMGCR
inhibition
MVK
PMVK
sterols, isoprenoids
HCT116
HMGCS1-FKBP12 K/I
UT
dTAGv1
HG
Statin
RhoA
(unprenylated)
HMGCS1
HMG
HMGCR
tubulin
24
72
240
93
57
B
HCT116 HMGCS1-FKBP12 Knock-in cells
UT
dTAGv1
(24h)
Hymeglusin
(24h)
Simvastatin
(24h)
x 4
16-plex TMTpro proteome quant
C
WT
dTAGv1
HG
Statin
Rep1
Rep2
Rep3
Rep4
HMGCS1
HMGCR
72
93
D
± 2 fold change
HCT116
MVK
HMGCR
APP
SQLE
PCSK9
MFGE8
VGF
HMGCS1
HIF1A
LDLR
IGFBP6
FGF19
FGFBP1
MYO15B
RAB12
DEPDC1
CDC20
DEPDC1B
RAB20
BCL2L12
MIEN1
PLK1
FBXO10
RAB29
n=9881 proteins
-Log10(p-value)
Log2(HG/UT, 24h)
E
lysosome
extracellular exosome
endoplasmic reticulum lumen
Golgi apparatus
cell surface
extracellular space
n = 10
n = 38
n = 15
n = 23
n = 19
n = 55
Upregulated
(n = 168)
- log (p-value)
F
UT
dTAG
HG
Statin
R1
R2
R3
R4
HMGCS1
HMGCR
MVD
MVK
MVP
IDI1
FDPS
FDFT1
GGPS1
SQLE
LSS
CYP51A1
MSMO1
NSDHL
SC5D
HSD17B7
HSD17B7
DHCR24
DHCR7
log2 fold-change
G
RHOBTB3
RHOD
RHOF
RHOG
RAB12
RAB20
RAB25
RAB28
RAB29
RAB33B
RAB38
RAB8A
RAB8B
RAC1
RAC2
RHOA
RHOB
RAB11A
RAB43
RAB5A
RAB5B
log2 fold-change

466 **FIGURE 3. Perturbing HMGCS1 by Hymeglusin and HMGCR by Simvastatin leads to identical global**
467 **proteome changes.**
468 (A) left panel: A schematic illustrating the mevalonate pathway flux. Three perturbation approaches—
469 inhibition or degradation of HMGCS1 and inhibition of HMGCR—are compared for their effects on global
470 proteome changes. Right panel: HCT116 HMGCS1-FKBP12^{F36V} knock-in cells were treated with dTAGv1
471 (100 nM, for HMGCS1 degradation), Hymeglusin (5 μM, for HMGCS1 inhibition), and Simvastatin (10 μM,
472 for HMGCR inhibition) for 48 hours. The cell extracts were then probed with the indicated antibodies to
473 check the cellular response.
474 (B) The 16-plex TMTpro approach was utilized to compare the global proteome changes after 24 hours of
475 the specified small molecule treatment.
476 (C) HEK293T cells treated as described in panel B were probed with the indicated antibodies as a quality
477 control step prior to proteomic analysis.
478 (D) Analysis of the TMT-plex data is presented as a volcano plot of the —$\log_{10}$-transformed p-value versus
479 the $\log_2$-transformed ratio of Hymeglusin treated/untreated (UT) conditions for HCT116 HMGCS1-
480 FKBP12^{F36V} knock-in cells. p values were calculated by two-sided Welch's t-test (adjusted to 1% FDR for
481 multiple comparisons). A total of 9881 proteins were quantified. n = 4 biological replicates.
482 (E) Gene ontology analyses of the statistically significant upregulated proteins (168 proteins) with more
483 than 2-fold changes are shown. N represents the number of proteins counted in the category.
484 (F) 19 quantified proteins in the mevalonate/sterol pathway were curated and their log2 fold-changes are
485 presented as a heat map. dTAG treatment led to the steep depletion of HMGCS1.
486 (G) Representative families of isoprenylation targets (Rho, Rab, Rheb, and Ras proteins) were curated from
487 1,200 statistically significant hits and plotted as a heatmap. No Ras or Rheb proteins showed statistically
488 significant change upon treatment.
489

Figure 4.

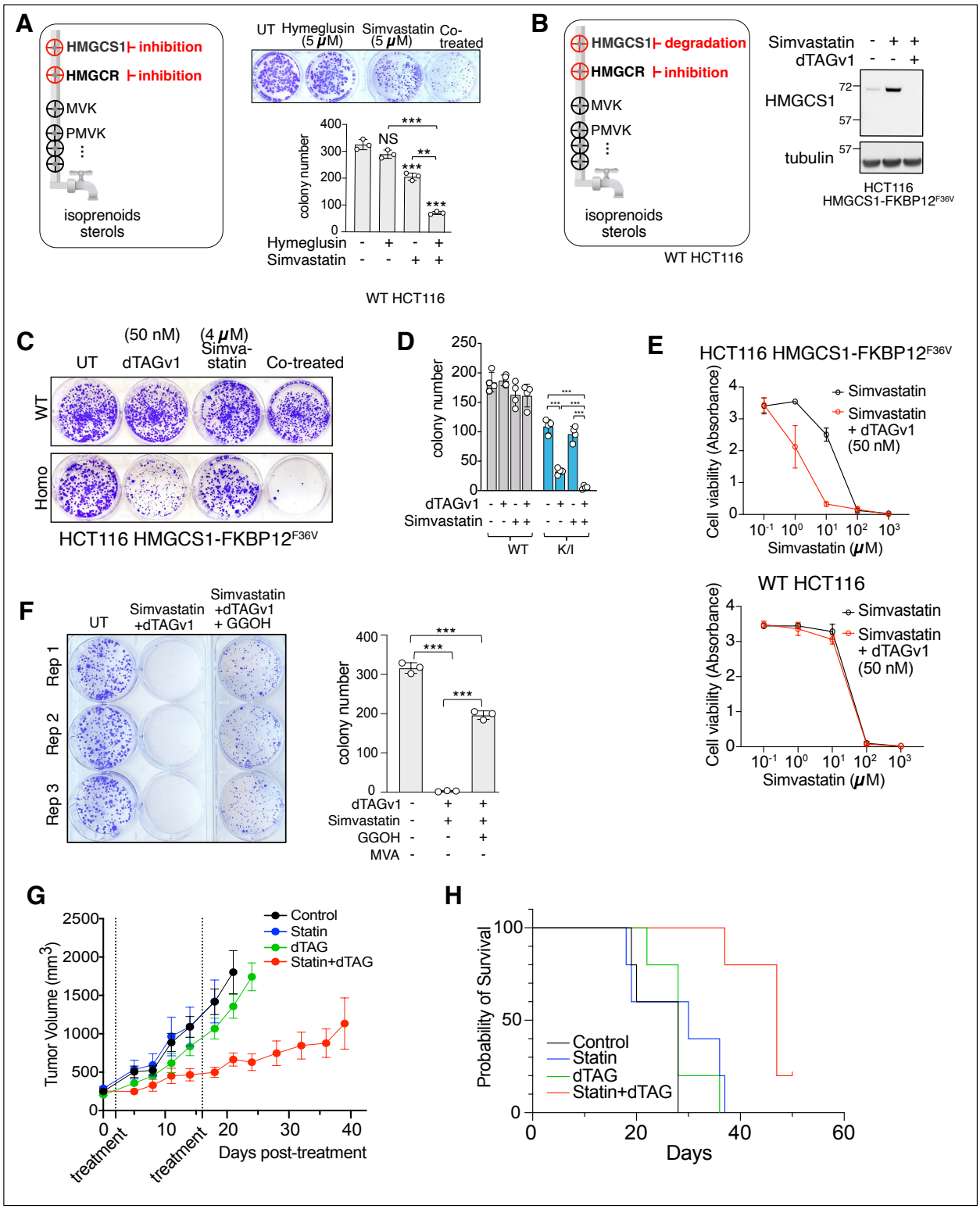
A
HMGCS1 inhibition
HMGCR inhibition
MVK
PMVK
isoprenoids
sterols
UT
Hymeglusin (5 μM)
Simvastatin (5 μM)
Co-treated
colony number
NS
Hymeglusin
Simvastatin
WT HCT116
B
HMGCS1 degradation
HMGCR inhibition
MVK
PMVK
isoprenoids
sterols
WT HCT116
Simvastatin
dTAGv1
HMGCS1
tubulin
HCT116
HMGCS1-FKBP12F36V
C
UT
(50 nM) dTAGv1
(4 μM) Simva-statin
Co-treated
WT
Homo
HCT116 HMGCS1-FKBP12F36V
D
colony number
dTAGv1
Simvastatin
WT
K/I
E
HCT116 HMGCS1-FKBP12F36V
Cell viability (Absorbance)
Simvastatin
Simvastatin + dTAGv1 (50 nM)
Simvastatin (μM)
WT HCT116
F
UT
Simvastatin +dTAGv1
Simvastatin +dTAGv1 + GGOH
Rep 1
Rep 2
Rep 3
colony number
dTAGv1
Simvastatin
GGOH
MVA
G
Tumor Volume (mm3)
Control
Statin
dTAG
Statin+dTAG
treatment
treatment
Days post-treatment
H
Probability of Survival
Control
Statin
dTAG
Statin+dTAG
Days

495 **FIGURE 4. Combinatory targeting HMGCS1 and HMGCR exhibit synergistic anti-tumor effects.**
496 (A) The left panel presents a schematic illustration of the combinatorial inhibition of HMGCS1 and HMGCR.
497 In the right panel, the colony formation assay results for HMGCS1-FKBP12^{F36V} K/I HCT116 cells are shown,
498 where treatments involved either Hymeglusin (5 μM), Simvastatin (5 μM), or a combination of both
499 inhibitors. Corresponding inhibitors were applied on days 5 and 7 after seeding, and the colony numbers
500 were counted on day 12. The accompanying quantification graph displays the means ± SD from biological
501 triplicates.
502 (B) The left panel illustrates the degradation of HMGCS1 and the inhibition of HMGCR as a combinatorial
503 approach to target the mevalonate pathway. The right panel shows the induction of HMGCS1 following
504 Simvastatin treatment, which was completely reversed by dTAGv1 treatment due to the induced
505 degradation in HCT116 cells expressing endogenous HMGCS1-FKBP12^{F36V}.
506 (C) HMGCS1 degradation by dTAGv1 (50 nM) increases the inhibitory effects of Simvastatin (4 μM) on the
507 colony-forming activity of HCT116 HMGCS1-FKBP12^{F36V} cells.
508 (D) Means ± s.d. of biological quadruplicate data from Panel C.
509 (E) HMGCS1 degradation by the dTAG system reduces the IC_{50} value of Simvastatin by 10-fold in HCT116
510 HMGCS1-FKBP12^{F36V} knock-in cells (top). Cell viability was assessed 24 hours after treating the
511 corresponding cells with increasing concentrations of Simvastatin and dTAGv1 (50 nM). The wild-type
512 HCT116 did not show the synergistic effect of dTAGv1 and Simvastatin (bottom).
513 (F) The anti-colony formation effect induced by the HMGCS1 degradation and HMGCR inhibition was
514 rescued by supplementation of geranylgeraniol (GGOH, 40 μM). HCT116 HMGCS1-FKBP12^{F36V} K/I cells
515 were treated with dTAGv1 (50 nM) and Simvastatin (4 μM) on days 5 and 7, post-seeding. GGOH (40 μM)
516 was added to the media of the corresponding cells on days 5 and 7. Means ± s.d. of biological triplicate
517 data is shown on the right.
518 (G) HMGCS1-FKBP12^{F36V} K/I HCT116 cells were implanted into nude mice. When the tumor size reached
519 200 – 250 mm^3, we administrated two treatment regimens (shown in dotted vertical lines), including saline
520 control, 5 mg/kg Simvastatin via gavage three times a week, weekly 5mg/kg dTAGv1 through i.p., and the
521 combination of both dTAGv1 and Simvastatin. Degradation of HMGCS1 by the dTAG system potentiates
522 the tumor growth-suppressing effect of Simvastatin. n = 5 mice for each condition.
523 (H) Survival probability analysis of the mice presented in Panel H using Kaplan-Meier software reveals
524 extended mortality in the dTAG and Statin co-treatment groups compared to the other control groups.

Figure 5

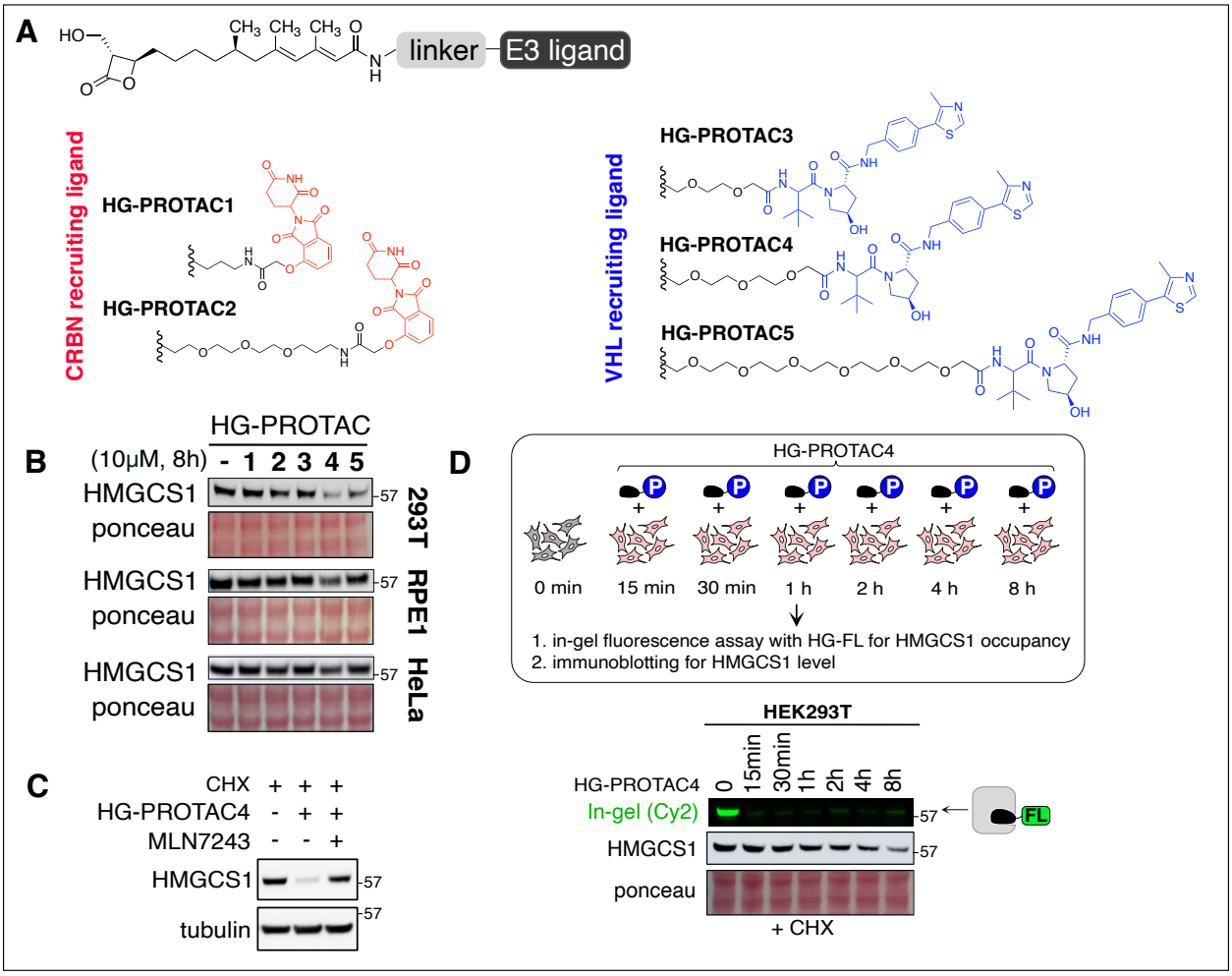

FIGURE 5. Development of bifunctional molecules that both inhibit and degrade HMGCS1.
(A) A framework of the Hymeglusin-PROTAC molecules is shown at the top. Structures of the five synthesized Hymeglusin-PROTAC candidates are displayed at the bottom. The CRBN-recruiting ligand or the VHL-recruiting ligand was conjugated using different linkers.
(B) HEK293T, RPE1, or HeLa cells were treated with each HG-PROTAC molecule (10 μM) for 8 hours. Cycloheximide (1 μM) was added to decouple the protein degradation from synthesis.
(C) HEK293T cells were treated with HG-PROTAC4 (10 μM, 16 h) in the presence or absence of ubiquitin-activating E1 enzyme inhibitor, MLN7243 (100 nM, 16 h).
(D) HG-PROTAC4-treated HEK293T cells in the presence of cycloheximide (1 μM) were collected at the indicated time points, and the lysates were treated with HG-FL to measure the occupancy of the catalytic cysteine of HMGCS1. After in-gel fluorescence analysis, the gel was processed to measure HMGCS1 levels by immunoblotting. Ponceau is shown as a loading control.

Figure 6

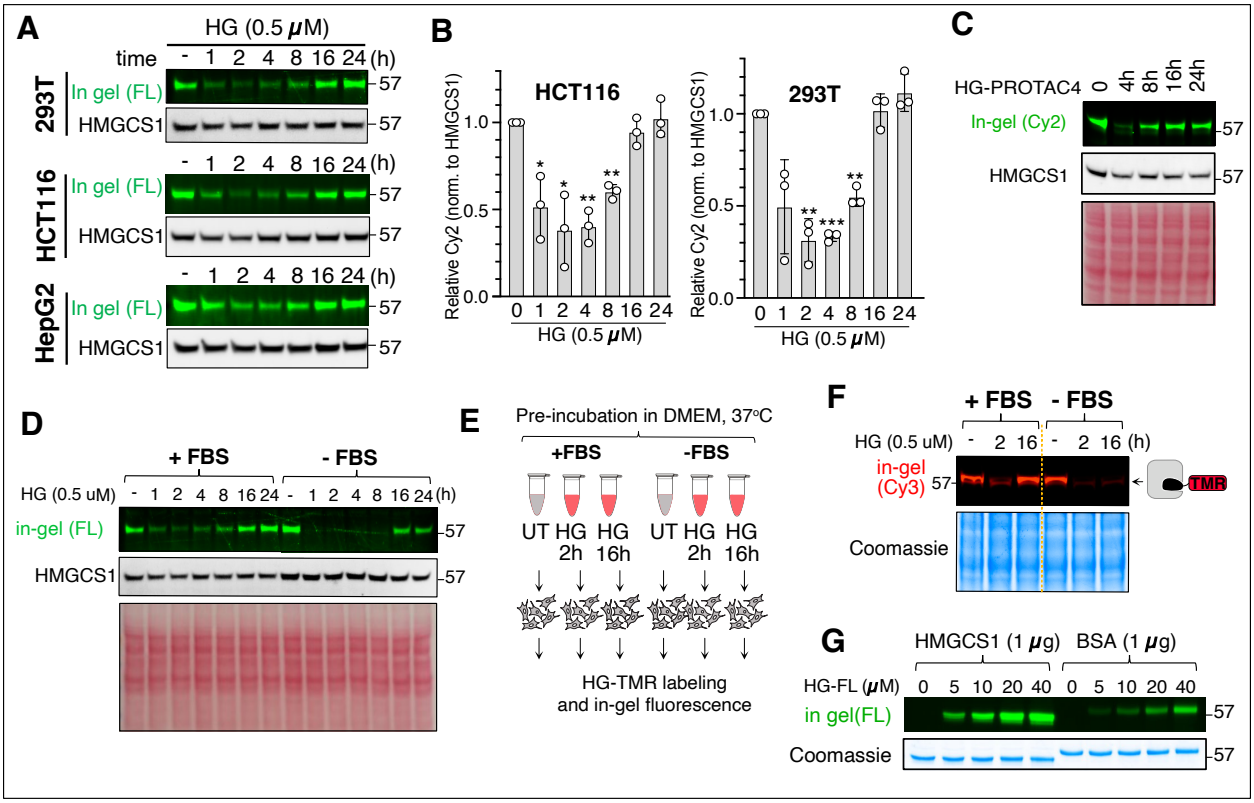

FIGURE 6. Hymeglusin exhibits poor serum stability.

(A) HCT116, HEK293T, and HepG2 cells were treated with Hymeglusin (0.5 μM) for the indicated time points, followed by lysis and reaction with the HG-FL probe. In-gel fluorescence analysis and immunoblotting were then performed

(B) The quantification of relative fluorescence intensity from three replicate experiments in panel A is presented. Mean ± s.d.

(C) HEK293T cells were treated with HG-PROTAC4 (5 μM) for the indicated time, followed by in-gel fluorescence analysis for HG-FL labeling and immunoblotting for assessing HMGCS1 level.

(D) The absence of FBS in the cell culture media delays the appearance of active HMGCS1 with free catalytic cysteine after prolonged treatment of cells with Hymeglusin.

(E) A workflow to test the effect of fetal bovine serum (FBS) on the stability of Hymeglusin. 0.5 μM of Hymeglusin was added to DMEM supplemented with or without 10% FBS. The media was then incubated at 37°C for 2 or 16 hours before being added to HEK293T cells.

(F) HEK293T cells treated as in panel E were subjected to in-gel fluorescence analysis.

(G) *In vitro* incubation of HG-FL with recombinant HMGCS1 (1 μg) or BSA (1 μg) for 1 hour produces a green fluorescence signal in the relevant molecular weight regions, indicating a strong interaction between HG-FL and BSA.

Figure S1

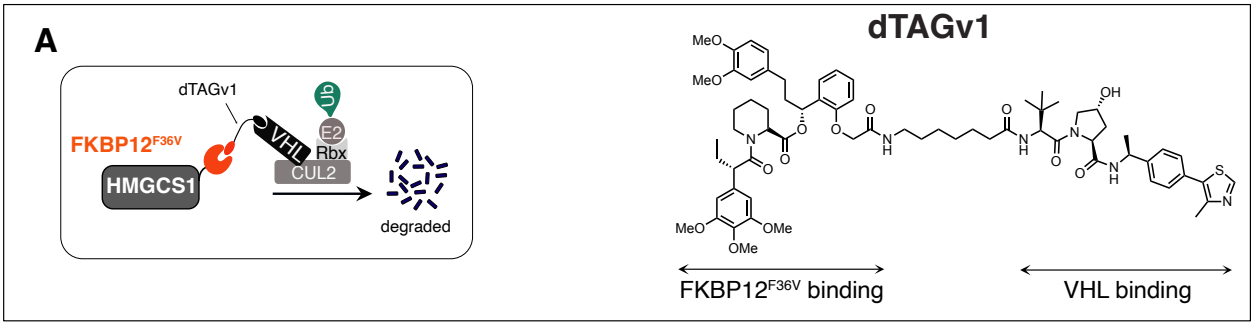

SI FIGURE 1. Overview of induced proteolysis by the dTAG system (Related to Figure 1).
(A) The schematic of the dTAG system (left) and chemical structure of the dTAGv1 ligand (right). This bifunctional ligand can bring VHL closer to the FKBP12^{F36V} mutant.

Figure S2

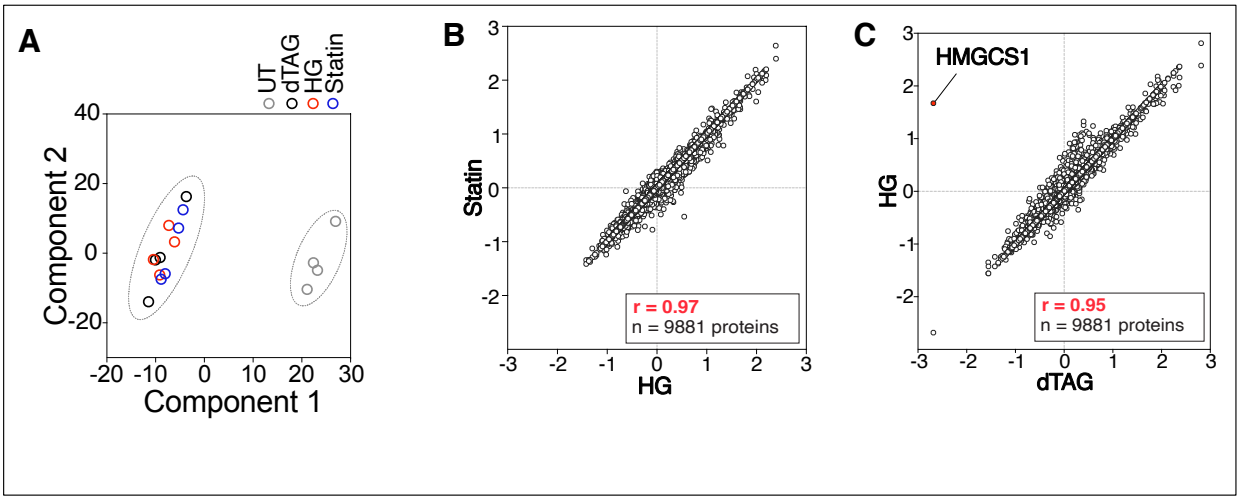

SI FIGURE 2. Global proteomic changes induced upon MVP inhibition (Related to Figure 3).
(A) Principal component analysis (PCA) of the total proteomics dataset, prepared as shown in Fig. 3B, indicates that dTAG, HG, and Statin-treated cells are grouped together.
(B,C) 9881 proteins were plotted for the $\log_2$-ratio of (Simvastatin/DMSO) against the $\log_2$-ratio of (HG/DMSO) for panel B, and $\log_2$-ratio of (Hymeglusin/DMSO) against the $\log_2$-ratio of (dTAGv1/DMSO) for panel C. N = 4 replicates. p values were calculated by two-sided Welch's t-test (adjusted to 1% FDR for multiple comparisons). A total of 9881 proteins were quantified. n = 4 biological replicates.

Figure S3

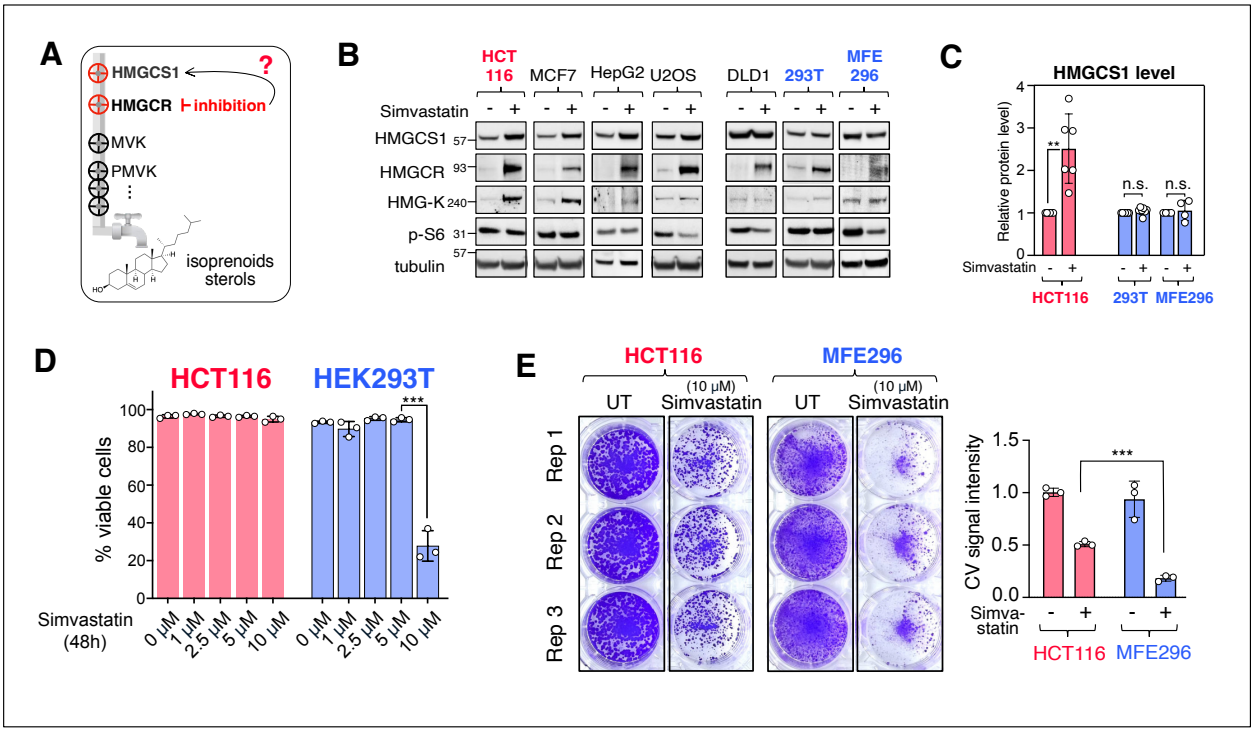

SI FIGURE 3. Relation between HMGCS1 upregulation and statin resistance (Related to Figure 4).
(A) A schematic showing the relationship between HMGCR inhibition and HMGCS1 up-regulation.
(B) The level of HMGCS1 upon Simvastatin treatment for 24 hours was assessed in seven different cell lines using immunoblotting analysis. Indicated cells were treated with Simvastatin (10 μM, 24h), followed by immunoblotting with indicated antibodies.
(C) The relative level of HMGCS1 protein was quantified from the experimental replicates shown in panel B, with n > 4 replicates. Mean ± s.d.
(D) Flow cytometry analysis of DAPI-stained versus unstained cells was conducted to evaluate cell viability after treating indicated cells with increasing concentrations of Simvastatin for 48 hours.
(E) Coloniformation assay with or without Simvastatin treatment was performed on MFE296 and HCT116 cell lines. The total signal intensity per plate, relative to the untreated condition, is presented on the right. Mean ± s.d. n = 3 replicates.

Figure S4

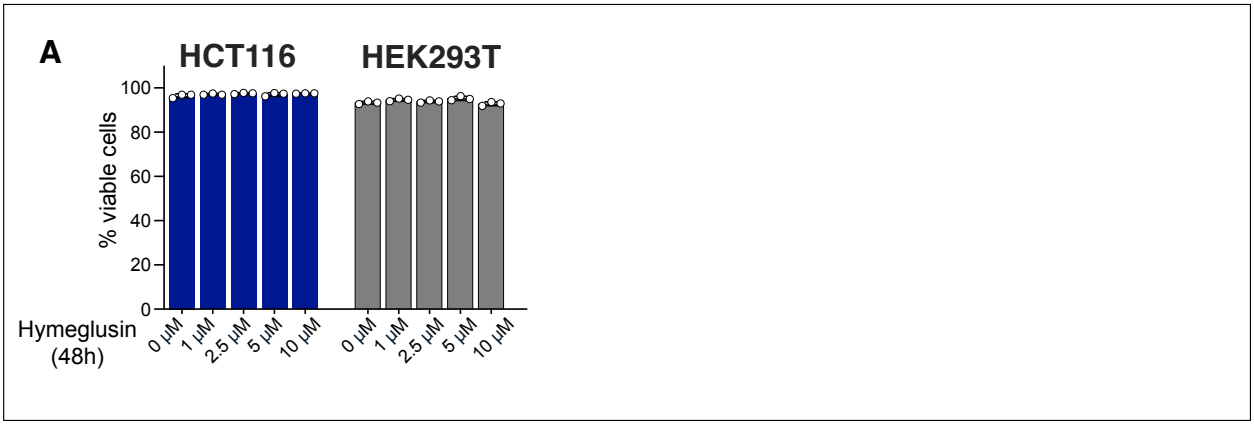

618
619
620 **SI FIGURE 4. Limited efficacy of Hymeglusin on cell proliferation (Related to Figure 6).**
621 (A) HEK293T and HCT116 cells were treated with increasing concentration of Hymeglusin, followed by cell
622 viability assay using flow-cytometry method.

623 **TABLE S1. AFFINITY-PROTEOMICS USING HYMEGLUSIN-BIOTIN PROBE (RELATED TO FIGURE**
624 **2).** HEK293T cells, pretreated with Hymeglusin or DMSO, were further treated with Hymeglusin-biotin,
625 followed by streptavidin enrichment and TMT-6plex analysis.

626 **TABLE S2. COMPARATIVE PROTEOMICS UPON MVP INHIBITION (RELATED TO FIGURE 3).** TMT-
627 based proteomic data for HCT116 HMGCS1-FKBP12^{F36V} cells following treatment with DMSO, dTAGv1,
628 Hymeglusin, and Simvastatin for 24 hours.

629

630

631

632

633

634

635

636

637

638

639

640

641

642

643 **STAR★METHODS**

644 **KEY RESOURCES TABLE**

Antibodies		
HMGCS1	Cell Signaling Technology	36877S; RRID:AB_2799107
HMGCR	Abcam	Ab242315
HMG-Lysine	Sigma-Aldrich	ABS2108
Tubulin, alpha	Abcam	Ab7291; RRID: AB_2241126
RhoA	Cell Signaling Technology	2117T; RRID: AB_10693922
Bacterial and virus strains		
E. coli DH5α	Enzynomics	CD011
Biological samples		
Chemicals, peptides, and recombinant proteins		
REVERTTM Total Protein Stain Kit	LI-COR	P/N926-11010
TCEP	Gold Biotechnology	TCEP10
EPPS	Sigma-Aldrich	E9502
2-Chloracetamide	Sigma-Aldrich	C0267
Protease inhibitor cocktail	Sigma-Aldrich	P8340

PhosSTOP	Sigma-Aldrich	4906845001
Hymeglusin	Cayman Chemical	11899
Simvastatin	Millipore Sigma	PHR1438
dTAGv1	Tocris Bioscience	6914
GGTI-298	Selleckchem	S7466
Crystal violet	Sigma-Aldrich	HT901-8FOZ
Critical commercial assays		
E.Z.N.A.® Plasmid DNA Mini Kit I	Omega Bio-tek	D6942-02
GeneJET Gel Extraction Kit	Thermo Scientific	K0692
Deposited data		
Experimental models: Cell lines		
Human: HEK293T	ATCC	CRL-3216; RRID:CVCL_0063
Human: HCT116	ATCC	CCL-247; RRID:CVCL_0291
Human: HeLa	ATCC	CCL-2; RRID:CVCL_0030
Human: RPE1	ATCC	CRL-4000; RRID:CVCL_4388
Human: HepG2	ATCC	HB-8065; RRID:CVCL_0027
Experimental models:Organisms/strains		
nu/nu athymic mice (Charles River Laboratory)		

Oligonucleotides		
Guide RNA sequence targeting C-terminus of HMGCS1: 5'-GAACATTAAGATACTCTGTG-3'	This paper	N/A
Recombinant DNA		
pSMART-HMGCS1-FKBP12 F36V-V5	This paper	N/A
Software and algorithms		
Prism 9	GraphPad	https://www.graphpad.com/scientific-software/prism
Image Lab 6.1	Bio-Rad Laboratories	https://www.bio-rad.com/en-us/product/image-lab-software?ID=KRE6P5E8Z
Perseus	Tyanova et al., Nat Methods. (2016) 13:731-40.	https://maxquant.net/perseus/
Other		
Orbitrap Eclipse Tribrid Mass Spectrometer	Thermo Fisher Scientific	FSN04-10000

645

RESOURCE AVAILABILITY

Lead contact

Further information and requests for resources and reagents should be directed to and will be fulfilled by lead contact Heeseon An, anh@mskcc.org

Materials availability

This study did not produce new materials.

Data and code availability

Any information analyzing the data reported in this study is available upon request from the lead contact.

EXPERIMENTAL MODEL AND STUDY PARTICIPANT DETAILS

Cell culture

HEK293T, HCT116, RPE1, HeLa, and HepG2 cells were grown in Dulbecco's modified Eagle's medium (DMEM), supplemented with 10% fetal bovine serum and maintained in a 5% CO_2 incubator at 37ºC.

Cell lysis and immunoblotting assay

Cells were plated 24 h before being treated with inhibitors or starvation medium, and cell confluency did not exceed 70% at the time of harvest. Cell pellets were lysed with either in-house RIPA buffer (50 mM HEPES, 150 mM NaCl, pH 7.6, 1% NP-40, 1% sodium deoxycholate, 0.1% SDS, 10 mM glycerophosphate, 10 mM sodium pyrophosphate, protease inhibitor cocktail, phosphatase inhibitor cocktail) containing 200 μM TCEP, 15 mM $MgCl_2$, and benzonase (Millipore, for RIPA only) or 0.5 % NP40 buffer (50 mM HEPES HCl, 150 mM NaCl, pH 7.4) containing protease inhibitors, phosphatase inhibitors, and 200 μM TCEP. Lysates in RIPA buffer were then sonicated, whereas lysates in NP40 buffer were pipetted and centrifuged at 7,000 rpm for 1 min without sonication. Bradford assay was performed to measure the protein concentration, and the normalized cell lysates were denatured by adding LDS supplemented with 50 mM DTT, followed by boiling at 90 ºC for 5 minutes. Less than 30 µg of each lysate was loaded onto the 4-12% NuPAGE Bis-Tris gel (Thermo Fisher Scientific), followed by SDS-PAGE with MES running buffer. Following transfer to PVDF membranes (0.45 µm or 0.2 µm, Millipore), blocking was performed with 5% non-fat milk at room temperature for 15 min, then incubated with primary antibodies overnight at 4ºC. After the incubation with primary antibobies, membranes were washed with TBST and further incubated with fluorescent IRDye antibody (1:20000) for 1 h at room temperature. The membrane was then imaged using OdysseyCLx (Licor) imager or Chemidoc MP (Biorad).

Total proteomics analysis using TMTpro

The total proteomics analyses were performed based on the previously reported method.[22] Briefly, cells are plated into a 10 cm dish per condition, a total of 16 dishes. 24 h later, dTAGv1 (100 nM), Hymeglusin (5 µM), or Simvastatin (10 µM) were added to cells and incubated for 24 h. Cells were then washed with ice-cold PBS five times and lysed with 800 µl of RIPA buffer (50 mM HEPES, 150 mM NaCl, pH 7.6, 1% NP-40, 1% sodium deoxycholate, 0.1% SDS, 10 mM glycerophosphate, 10 mM sodium pyrophosphate, protease inhibitor cocktail, Phosphatase inhibitor cocktail, pH 7.5). The lysate was then collected and sonicated three times, followed by Bradford assay to measure the protein concentration. The total protein concentration was adjusted to become 3 mg/ml throughout the samples using RIPA buffer. 125 µg of each protein extract was taken and reduced by incubation in the presence of 5 mM TCEP at 55 ºC for 10 min. After cooling down to room temperature, the lysates were reacted with chloroacetamide solution (final conc. 20 mM) at room temperature for 15 min, followed by chloroform/methanol precipitation. Protein discs were resuspended in 100 mM EPPS (pH 8.5) containing 0.1% RapiGest and digested at 37 ºC overnight with Trypsin (100:1 protein-to-protease ratio). 16-plex tandem mass tag labeling of each sample was performed by adding 10 µL of the 20 ng/mL stock of TMTpro reagent along with acetonitrile to achieve a final acetonitrile concentration of approximately 30% (v/v). Following incubation at room temperature for 1 h, the reaction was quenched with hydroxylamine to a final concentration of 1% (v/v) for 15 min. The TMTpro-

699 labeled samples were pooled together at a 1:1 ratio. The sample was vacuum centrifuged to near dryness
700 and subjected to C18 solid-phase extraction (SPE) (50 mg, Sep-Pak, Waters). Dried TMTpro-labeled
701 sample was resuspended in 100 μL of 10 mM NH_4HCO_3 pH 8.0 and fractionated using BPRP HPLC. Briefly,
702 samples were offline fractionated over a 90 min run into 96 fractions by high pH reverse-phase HPLC
703 (Agilent LC1260) through an aeris peptide xb-c18 column (Phenomenex; 250 mm x 3.6 mm) with mobile
704 phase A containing 5% acetonitrile and 10 mM NH_4HCO_3 in LC-MS grade H_2O, and mobile phase B
705 containing 90% acetonitrile and 10 mM NH4HCO3 in LC-MS grade H_2O (both pH 8.0). The 96 resulting
706 fractions were then pooled in a non-continuous manner into 24 fractions (as outlined in Figure S5 of Paulo
707 et al., 2016)[49] for mass spectrometry analysis. Fractions were vacuum centrifuged to near dryness. Each
708 consolidated fraction was desalted via Stage Tip, dried again via vacuum centrifugation, and reconstituted
709 in 5 % acetonitrile, 1 % formic acid for LC-MS/MS processing.
710
711 Mass spectrometry data were acquired using an Orbitrap Eclipse Tribrid mass spectrometer (Thermo Fisher
712 Scientific, San Jose, CA) connected to an UltiMate 3000 RSLCnano system liquid chromatography (LC)
713 pump (Thermo Fisher Scientific, San Jose, CA). Peptides were separated on a 100 µm inner diameter
714 microcapillary column packed in-house with ~ 30 cm of HALO Peptide ES-C18 resin (2.7 µm, 160 Å,
715 Advanced Materials Technology, Wilmington, DE) with a gradient consisting of 5 %–23 % (0-75 min), 23-
716 40 % (75-110 min) (ACN, 0.1% FA) over a 120 min run at ~500 nL/min. 3/10 of each fraction was loaded
717 onto the column for analysis. Proteome analysis used Multi-Notch MS^3-based TMT quantification, combined
718 with Real Time Search analysis software, and the FAIMS Pro Interface (using previously optimized 3 CV
719 parameters), to reduce ion interference. The scan sequence began with an MS^1 spectrum (Orbitrap
720 analysis; resolution 120,000 at 200 Th; mass range 400−1500 m/z; maximum injection time 50 ms;
721 automatic gain control (AGC) target $4x10^5$). For MS2 analysis, precursors were selected based on a cycle
722 time of 1.25 sec/CV method (FAIMS CV=-40/-60/-80). MS^2 analysis consisted of collision-induced
723 dissociation (quadrupole ion trap analysis; Rapid scan rate; AGC $1.0x10^4$; isolation window 0.5 Th;
724 normalized collision energy (NCE) 35; maximum injection time 35 ms). Monoisotopic peak assignment was
725 used, and previously interrogated precursors were excluded using a dynamic window (180 s ±10 ppm).
726 Following the acquisition of each MS^2 spectrum, a synchronous-precursor-selection (SPS) API-MS^3 scan
727 was collected on the top 10 most intense ions b or y-ions matched by the online search algorithm in the
728 associated MS^2 spectrum. MS^3 precursors were fragmented by high energy collision-induced dissociation
729 (HCD) and analyzed using the Orbitrap (NCE 45; AGC $2.5x10^5$; maximum injection time 200 ms, resolution
730 was 50,000 at 200 Th). Closeout was set at two peptides per protein per fraction, so that MS^3s were no
731 longer collected for proteins having two peptide spectrum matches (PSMs) that passed quality filters.
732
733 **Proteomics Data Analysis**
734 Mass spectra were processed using a Comet-based (2020.01 rev. 4) software pipeline [50,51]. Spectra were
735 first converted to mzXML and monoisotopic peaks were re-assigned using Monocle software [52]. MS^2
736 spectra were matched with peptide sequences with a composite sequence database including the Human
737 Reference Proteome (2020-01 - SwissProt entries only) UniProt database, as well as sequences of
738 common contaminants. This database was concatenated with one composed of all protein sequences in
739 the reversed order. Analysis was performed using a 50 ppm precursor ion tolerance. Static modifications
740 included TMTpro tags on lysine residues and peptide N termini (+304.207 Da) and carbamidomethylation
741 of cysteine residues (+57.021 Da). Oxidation of methionine residues (+15.995 Da) was set as a variable
742 modification. Peptide-spectrum matches (PSMs) were adjusted to a 1% false discovery rate (FDR) [53]. PSM
743 filtering was performed using a linear discriminant analysis, [54], while considering the following parameters:
744 Comet log expect, different sequence delta Comet log expect, missed cleavages, peptide length, charge
745 state, precursor mass accuracy, and fraction of ions matched. For protein-level comparisons, PSMs were
746 identified, quantified, and collapsed to a 1% peptide false discovery rate (FDR) and then collapsed further
747 to a final protein-level FDR of 1% [55]. To generate the smallest set of proteins required to account for all
748 observed peptides, the principles of parsimony were applied. For TMTpro-based reporter ion quantitation,
749 the summed signal-to-noise (S:N) ratio for each TMT channel was first extracted based on the closest
750 matching centroid to the expected mass of the TMT reporter ion (integration tolerance of 0.003 Da). Isotopic
751 impurities of the different TMTpro reagents provided by the manufacturer specifications, were used to adjust
752 reporter ion intensities. Proteins were quantified by summing reporter ion signal-to-noise measurements
753 across all matching PSMs, resulting in a ‘‘summed signal-to-noise’’ measurement. For total proteome,
754 PSMs with poor quality, or isolation specificity less than 0.75, or with TMT reporter summed signal-to-noise

755 ratio that were less than 160 or had no MS^3 spectra were excluded from quantification. For phospho
756 proteome, PSMs with poor quality, MS^2 spectra with 13 or more TMT reporter ion channels missing, or
757 isolation specificity less than 0.8, or with TMT reporter summed signal-to-noise ratio that were less than
758 160 were excluded from quantification. The AScore algorithm was used to determine the localization of
759 phosphorylation sites [56]. AScore is a probability-based approach for high-throughput protein
760 phosphorylation site localization. Precisely, a threshold of 13 relates to 95% confidence in site localization.
761 Protein quantification values were exported for further analysis in Microsoft Excel and Perseus [57]. Each
762 reporter ion channel was summed across all quantified proteins and normalized, assuming equal protein
763 loading was achieved for all samples. The maximum and minimum TMT ratio quantifiable was capped at
764 100-fold. Organellar protein marker annotations were compiled using the proteins that had scored with
765 confidence ''very high'' or ''high'' from a previously published HeLa dataset [58] and additional entries from
766 manually curated literature.
767
768 Supplemental data tables list all quantified proteins and the TMTpro reporter ratio associated with control
769 channels used for quantitative analysis.
770
771 **IP-MS analysis using Hymeglusin-biotin probe**
772 HEK293T cells were seeded overnight before incubating with media containing 5 μM hymeglusin or vehicle
773 control (DMSO) for 0.5 hrs. Then 5 μM Hymeglusin-biotin was introduced to the cells and incubated for
774 additional 2 hrs. Cells were washed with ice-cold PBS three times. The cells were then lysed with 200 μl of
775 HEPES-NP40 buffer (50 mM HEPES, 150 mM NaCl, pH 7.5, 0.25%NP40). The lysate was centrifuged at
776 7k for 1 min, and the supernatant was collected. The supernatant was then reduced by 5 mM TCEP (10 min,
777 room temperature) and alkylated by chloroacetamide (20 mM final concentration, 15 min, room
778 temperature). $MeOH/CHCl_3$ precipitation was followed to remove any remaining Hymeglusin-biotin in the
779 cell lysates. The white protein disk was then resuspended in 2% SDS (50 mM HEPES 150 mM NaCl, pH7.2,
780 2.5 mM TCEP) and sonicated once with a tip sonicator and then diluted in HEPES-NP40 buffer (final SDS
781 concentration is < 0.5%). Subsequently, 10 μl of high-capacity streptavidin was added to the cell lysates
782 and incubated for 2 hours at room temperature. Flow-through was then stored for the quality control
783 immunoblots, and the beads were washed with RIPA X 2, 2%SDS X 3, RIPA X 2, and PBS X 3. The beads
784 were transferred onto hydrophilic PTFE membrane filter cups and washed twice with water. Completely
785 dried beads were then resuspended in 50 μl of hexafluoroisopropanol (HFIP), incubated for 5 min with
786 shaking, and eluted by spinning at 5k rpm. 50 μl of HFIP was added to the beads again, and the eluates
787 were combined and dried in speed vac for ~10 min. Then, 6-plex TMT labeling was performed as described
788 in the proteomics sample preparation section.
789
790 **In-gel fluorescent analysis with HG-fluorescence probes**
791 Recombinant HMGCS1 protein (1 ug) or cell lysates were incubated with 5 μM Hymeglusin-FITC (HG-FL)
792 or Hymeglusin-TMR (HG-TMR) probe at 37°C for 1 h. The labeling reaction was stopped by adding 4X
793 LDS containing DTT and boiling at 90°C for 5 m. The samples were subjected to SDS-PAGE, and the
794 fluorescent signal in the gel was detected by Chemidoc MP (Biorad).
795
796 **Cell viability assay**
797 Cells viability was evaluated using WST1-based colorimetric assay (Roche). 2 x 10^4 cells in 100 μl of culture
798 medium were seeded for each well of 96 well plates. Next day, the cells were treated with culture media
799 containing various amounts of simvastatin and 50 nM of dTAGv1. After 24 h, cells were incubated with
800 WST-1 solution, which was diluted to 1:10 with culture medium in the cell culture incubator. After 4 h, the
801 absorbance of samples was measured using a microplate reader. The wavelength to measure the
802 absorbance of formazan product from viable cells was 450 nm, and the reference wavelength was 690 nm.
803
804 **Colony formation assay**
805 To evaluate the ability of single cancer cells to form a colony, cells were plated at a concentration of 1,500
806 cells/well onto 6 well plates (day 0). At day 5 and day 7, the cells were treated with the corresponding
807 chemicals. On day 12, the cells were stained with a crystal violet working solution, which contains 0.5%
808 crystal violet and 4% paraformaldehyde in PBS. Numbers of colonies were counted for each well (n = 2 or
809 3) and presented as mean ± s.d.

Animal Experiments

Animal experiments were performed in compliance with protocols approved by the Research Animal Resource Center and Institutional Animal Care and Use Committee at Memorial Sloan Kettering Cancer Center. 20 Athymic nude mice (nu/nu athymic mice, Charles River Laboratory) were implanted with HCT116 HMGCS1-FKBP12^{F36V} homozygous knock-in (KI) cells through subcutaneous injection of 2 x 10^6 cells per mouse. The treatment was initiated as the tumor size became 200-250 mm^3. Four groups of mice were administered with two treatment regimens over a two-week interval, including saline control, 5mg/kg Simvastatin three times per week via oral gavage, 5 mg/kg dTAGv1 weekly via intraperitoneally injected (IP), and the combination of both Simvastatin and dTAGv1. PBS is used as a vehicle for both simvastatin and dTAGv1. Tumor growth was monitored and recorded twice a week for 40 days, and five mice were used per condition.

Quantification and statistical analysis

P values in the volcano plots of the proteomics data were analyzed by two-sided Welch's t-test which was adjusted for multiple comparisons. Comparisons of the quantified data (immunoblotting, colony formation, tumor spheroids) were performed by unpaired Student's t-test; Statistical significance was judged based on p-values; *$p < 0.05$; **$p < 0.01$; ***$p < 0.001$.

REFERENCES

1. Brown, M.S., and Goldstein, J.L. (1986). A receptor-mediated pathway for cholesterol homeostasis. Science *232*, 34-47. 10.1126/science.3513311.

2. Goldstein, J.L., and Brown, M.S. (1990). Regulation of the mevalonate pathway. Nature *343*, 425-430. 10.1038/343425a0.

3. Luo, J., Yang, H., and Song, B.L. (2020). Mechanisms and regulation of cholesterol homeostasis. Nat Rev Mol Cell Biol *21*, 225-245. 10.1038/s41580-019-0190-7.

4. Mullen, P.J., Yu, R., Longo, J., Archer, M.C., and Penn, L.Z. (2016). The interplay between cell signalling and the mevalonate pathway in cancer. Nat Rev Cancer *16*, 718-731. 10.1038/nrc.2016.76.

5. Juarez, D., and Fruman, D.A. (2021). Targeting the Mevalonate Pathway in Cancer. Trends Cancer *7*, 525-540. 10.1016/j.trecan.2020.11.008.

6. Clendening, J.W., Pandyra, A., Boutros, P.C., El Ghamrasni, S., Khosravi, F., Trentin, G.A., Martirosyan, A., Hakem, A., Hakem, R., Jurisica, I., and Penn, L.Z. (2010). Dysregulation of the mevalonate pathway promotes transformation. Proc Natl Acad Sci U S A *107*, 15051-15056. 10.1073/pnas.0910258107.

7. Jiang, P., Mukthavaram, R., Chao, Y., Nomura, N., Bharati, I.S., Fogal, V., Pastorino, S., Teng, D., Cong, X., Pingle, S.C., et al. (2014). In vitro and in vivo anticancer effects of mevalonate pathway modulation on human cancer cells. Br J Cancer *111*, 1562-1571. 10.1038/bjc.2014.431.

8. Kuzu, O.F., Noory, M.A., and Robertson, G.P. (2016). The Role of Cholesterol in Cancer. Cancer Res *76*, 2063-2070. 10.1158/0008-5472.CAN-15-2613.

9. Karlic, H., Thaler, R., Gerner, C., Grunt, T., Proestling, K., Haider, F., and Varga, F. (2015). Inhibition of the mevalonate pathway affects epigenetic regulation in cancer cells. Cancer Genet *208*, 241-252. 10.1016/j.cancergen.2015.03.008.

853 10. Zhou, C., Li, J., Sun, X., Zhao, L., Zhan, H., Liang, H., Fang, P., Zhang, T., He, Q., Du, J., and
854 Zeng, H. (2024). Targeting HMGCS1 restores chemotherapy sensitivity in acute myeloid leukemia.
855 Blood Sci *6*, e00192. 10.1097/BS9.0000000000000192.

856 11. Pandyra, A.A., Mullen, P.J., Goard, C.A., Ericson, E., Sharma, P., Kalkat, M., Yu, R., Pong, J.T.,
857 Brown, K.R., Hart, T., et al. (2015). Genome-wide RNAi analysis reveals that simultaneous
858 inhibition of specific mevalonate pathway genes potentiates tumor cell death. Oncotarget *6*, 26909-
859 26921. 10.18632/oncotarget.4817.

860 12. Malhi, M., Norris, M.J., Duan, W., Moraes, T.J., and Maynes, J.T. (2021). Statin-mediated
861 disruption of Rho GTPase prenylation and activity inhibits respiratory syncytial virus infection.
862 Commun Biol *4*, 1239. 10.1038/s42003-021-02754-2.

863 13. Jiao, Z., Cai, H., Long, Y., Sirka, O.K., Padmanaban, V., Ewald, A.J., and Devreotes, P.N. (2020).
864 Statin-induced GGPP depletion blocks macropinocytosis and starves cells with oncogenic defects.
865 Proc Natl Acad Sci U S A *117*, 4158-4168. 10.1073/pnas.1917938117.

866 14. Whyte, D.B., Kirschmeier, P., Hockenberry, T.N., Nunez-Oliva, I., James, L., Catino, J.J., Bishop,
867 W.R., and Pai, J.K. (1997). K- and N-Ras are geranylgeranylated in cells treated with farnesyl
868 protein transferase inhibitors. J Biol Chem *272*, 14459-14464. 10.1074/jbc.272.22.14459.

869 15. Kohl, N.E., Mosser, S.D., deSolms, S.J., Giuliani, E.A., Pompliano, D.L., Graham, S.L., Smith, R.L.,
870 Scolnick, E.M., Oliff, A., and Gibbs, J.B. (1993). Selective inhibition of ras-dependent
871 transformation by a farnesyltransferase inhibitor. Science *260*, 1934-1937.
872 10.1126/science.8316833.

873 16. Philips, M.R., and Cox, A.D. (2007). Geranylgeranyltransferase I as a target for anti-cancer drugs.
874 J Clin Invest *117*, 1223-1225. 10.1172/JCI32108.

875 17. Ullah, N., Mansha, M., and Casey, P.J. (2016). Protein Geranylgeranyltransferase Type 1 as a
876 Target in Cancer. Curr Cancer Drug Targets *16*, 563-571. 10.2174/1568009616666151203224603.

877 18. Drake, M.T., Clarke, B.L., and Khosla, S. (2008). Bisphosphonates: mechanism of action and role
878 in clinical practice. Mayo Clin Proc *83*, 1032-1045. 10.4065/83.9.1032.

879 19. Lin, J.H. (1996). Bisphosphonates: a review of their pharmacokinetic properties. Bone *18*, 75-85.
880 10.1016/8756-3282(95)00445-9.

881 20. Jiang, W., Hu, J.W., He, X.R., Jin, W.L., and He, X.Y. (2021). Statins: a repurposed drug to fight
882 cancer. J Exp Clin Cancer Res *40*, 241. 10.1186/s13046-021-02041-2.

883 21. Longo, J., van Leeuwen, J.E., Elbaz, M., Branchard, E., and Penn, L.Z. (2020). Statins as
884 Anticancer Agents in the Era of Precision Medicine. Clin Cancer Res *26*, 5791-5800. 10.1158/1078-
885 0432.CCR-20-1967.

886 22. Yi, S.A., Sepic, S., Schulman, B.A., Ordureau, A., and An, H. (2024). mTORC1-CTLH E3 ligase
887 regulates the degradation of HMG-CoA synthase 1 through the Pro/N-degron pathway. Mol Cell
888 *84*, 2166-2184 e2169. 10.1016/j.molcel.2024.04.026.

889 23. Zhou, C., Wang, Z., Yang, S., Li, H., and Zhao, L. (2022). Hymeglusin Enhances the Pro-Apoptotic
890 Effects of Venetoclax in Acute Myeloid Leukemia. Front Oncol *12*, 864430.
891 10.3389/fonc.2022.864430.

892 24. Casselbrant, A., Elias, E., Hallersund, P., Elebring, E., Cervin, J., Fandriks, L., and Wallenius, V.
893 (2024). Intestinal Ketogenesis and Permeability. Int J Mol Sci *25*. 10.3390/ijms25126555.

894 25. Greenspan, M.D., Yudkovitz, J.B., Lo, C.Y., Chen, J.S., Alberts, A.W., Hunt, V.M., Chang, M.N.,
895 Yang, S.S., Thompson, K.L., Chiang, Y.C., and et al. (1987). Inhibition of hydroxymethylglutaryl-
896 coenzyme A synthase by L-659,699. Proc Natl Acad Sci U S A *84*, 7488-7492.
897 10.1073/pnas.84.21.7488.

898 26. Greenspan, M.D., Bull, H.G., Yudkovitz, J.B., Hanf, D.P., and Alberts, A.W. (1993). Inhibition of 3-
899 hydroxy-3-methylglutaryl-CoA synthase and cholesterol biosynthesis by beta-lactone inhibitors and
900 binding of these inhibitors to the enzyme. Biochem J *289 (Pt 3)*, 889-895. 10.1042/bj2890889.

901 27. Tomoda, H., Kumagai, H., Takahashi, Y., Tanaka, Y., Iwai, Y., and Omura, S. (1988). F-244
902 (1233A), a specific inhibitor of 3-hydroxy-3-methylglutaryl coenzyme A synthase: taxonomy of
903 producing strain, fermentation, isolation and biological properties. J Antibiot (Tokyo) *41*, 247-249.
904 10.7164/antibiotics.41.247.

905 28. Tomoda, H., Kumagai, H., Tanaka, H., and Omura, S. (1987). F-244 specifically inhibits 3-hydroxy-
906 3-methylglutaryl coenzyme A synthase. Biochim Biophys Acta *922*, 351-356.

907 29. Tomoda, H., Kumagai, H., Tanaka, H., and Omura, S. (1993). Specific binding of beta-lactone
908 1233A to 3-hydroxy-3-methylglutaryl-coenzyme A synthase. J Antibiot (Tokyo) *46*, 872-874.
909 10.7164/antibiotics.46.872.

910 30. Tomoda, H., Ohbayashi, N., Morikawa, Y., Kumagai, H., and Omura, S. (2004). Binding site for
911 fungal beta-lactone hymeglusin on cytosolic 3-hydroxy-3-methylglutaryl coenzyme A synthase.
912 Biochim Biophys Acta *1636*, 22-28. 10.1016/j.bbalip.2003.11.005.

913 31. Skaff, D.A., Ramyar, K.X., McWhorter, W.J., Barta, M.L., Geisbrecht, B.V., and Miziorko, H.M.
914 (2012). Biochemical and structural basis for inhibition of Enterococcus faecalis
915 hydroxymethylglutaryl-CoA synthase, mvaS, by hymeglusin. Biochemistry *51*, 4713-4722.
916 10.1021/bi300037k.

917 32. Shafqat, N., Turnbull, A., Zschocke, J., Oppermann, U., and Yue, W.W. (2010). Crystal structures
918 of human HMG-CoA synthase isoforms provide insights into inherited ketogenesis disorders and
919 inhibitor design. J Mol Biol *398*, 497-506. 10.1016/j.jmb.2010.03.034.

920 33. Pojer, F., Ferrer, J.L., Richard, S.B., Nagegowda, D.A., Chye, M.L., Bach, T.J., and Noel, J.P.
921 (2006). Structural basis for the design of potent and species-specific inhibitors of 3-hydroxy-3-
922 methylglutaryl CoA synthases. Proc Natl Acad Sci U S A *103*, 11491-11496.
923 10.1073/pnas.0604935103.

924 34. Trub, A.G., Wagner, G.R., Anderson, K.A., Crown, S.B., Zhang, G.F., Thompson, J.W., Ilkayeva,
925 O.R., Stevens, R.D., Grimsrud, P.A., Kulkarni, R.A., et al. (2022). Statin therapy inhibits fatty acid
926 synthase via dynamic protein modifications. Nat Commun *13*, 2542. 10.1038/s41467-022-30060-
927 w.

928 35. Wagner, G.R., Bhatt, D.P., O'Connell, T.M., Thompson, J.W., Dubois, L.G., Backos, D.S., Yang,
929 H., Mitchell, G.A., Ilkayeva, O.R., Stevens, R.D., et al. (2017). A Class of Reactive Acyl-CoA
930 Species Reveals the Non-enzymatic Origins of Protein Acylation. Cell Metab *25*, 823-837 e828.
931 10.1016/j.cmet.2017.03.006.

932 36. Nabet, B., Ferguson, F.M., Seong, B.K.A., Kuljanin, M., Leggett, A.L., Mohardt, M.L., Robichaud,
933 A., Conway, A.S., Buckley, D.L., Mancias, J.D., et al. (2020). Rapid and direct control of target
934 protein levels with VHL-recruiting dTAG molecules. Nat Commun *11*, 4687. 10.1038/s41467-020-
935 18377-w.

936 37. Jo, Y., and DeBose-Boyd, R.A. (2022). Post-Translational Regulation of HMG CoA Reductase.
937 Cold Spring Harb Perspect Biol *14*. 10.1101/cshperspect.a041253.

938 38. Medina, M.W., Theusch, E., Naidoo, D., Bauzon, F., Stevens, K., Mangravite, L.M., Kuang, Y.L.,
939 and Krauss, R.M. (2012). RHOA is a modulator of the cholesterol-lowering effects of statin. PLoS
940 Genet *8*, e1003058. 10.1371/journal.pgen.1003058.

941 39. Madison, B.B. (2016). Srebp2: A master regulator of sterol and fatty acid synthesis. J Lipid Res *57*,
942 333-335. 10.1194/jlr.C066712.

943 40. Pandyra, A., and Penn, L.Z. (2014). Targeting tumor cell metabolism via the mevalonate pathway:
944 Two hits are better than one. Mol Cell Oncol *1*, e969133. 10.4161/23723548.2014.969133.

945 41. Clendening, J.W., Pandyra, A., Li, Z., Boutros, P.C., Martirosyan, A., Lehner, R., Jurisica, I., Trudel,
946 S., and Penn, L.Z. (2010). Exploiting the mevalonate pathway to distinguish statin-sensitive multiple
947 myeloma. Blood *115*, 4787-4797. 10.1182/blood-2009-07-230508.

948 42. Longo, J., Mullen, P.J., Yu, R., van Leeuwen, J.E., Masoomian, M., Woon, D.T.S., Wang, Y., Chen,
949 E.X., Hamilton, R.J., Sweet, J.M., et al. (2019). An actionable sterol-regulated feedback loop
950 modulates statin sensitivity in prostate cancer. Mol Metab *25*, 119-130.
951 10.1016/j.molmet.2019.04.003.

952 43. Tomoda, H., Ohbayashi, N., Kumagai, H., Hashizume, H., Sunazuka, T., and Omura, S. (1999).
953 Differential inhibition of HMG-CoA synthase and pancreatic lipase by the specific chiral isomers of
954 beta-lactone DU-6622. Biochem Biophys Res Commun *265*, 536-540. 10.1006/bbrc.1999.1712.

955 44. Burslem, G.M., Smith, B.E., Lai, A.C., Jaime-Figueroa, S., McQuaid, D.C., Bondeson, D.P., Toure,
956 M., Dong, H., Qian, Y., Wang, J., et al. (2018). The Advantages of Targeted Protein Degradation
957 Over Inhibition: An RTK Case Study. Cell Chem Biol *25*, 67-77 e63.
958 10.1016/j.chembiol.2017.09.009.

959 45. Kiely-Collins, H., Winter, G.E., and Bernardes, G.J.L. (2021). The role of reversible and irreversible
960 covalent chemistry in targeted protein degradation. Cell Chem Biol *28*, 952-968.
961 10.1016/j.chembiol.2021.03.005.

962 46. Guo, W.H., Qi, X., Yu, X., Liu, Y., Chung, C.I., Bai, F., Lin, X., Lu, D., Wang, L., Chen, J., et al.
963 (2020). Enhancing intracellular accumulation and target engagement of PROTACs with reversible
964 covalent chemistry. Nat Commun *11*, 4268. 10.1038/s41467-020-17997-6.

965 47. Mishra, V., and Heath, R.J. (2021). Structural and Biochemical Features of Human Serum Albumin
966 Essential for Eukaryotic Cell Culture. Int J Mol Sci *22*. 10.3390/ijms22168411.

967 48. van der Vusse, G.J. (2009). Albumin as fatty acid transporter. Drug Metab Pharmacokinet *24*, 300-
968 307. 10.2133/dmpk.24.300.

969 49. Paulo, J.A., O'Connell, J.D., Everley, R.A., O'Brien, J., Gygi, M.A., and Gygi, S.P. (2016).
970 Quantitative mass spectrometry-based multiplexing compares the abundance of 5000 S. cerevisiae
971 proteins across 10 carbon sources. J Proteomics *148*, 85-93. 10.1016/j.jprot.2016.07.005.

972 50. Eng, J.K., Hoopmann, M.R., Jahan, T.A., Egertson, J.D., Noble, W.S., and MacCoss, M.J. (2015).
973 A deeper look into Comet--implementation and features. J Am Soc Mass Spectrom *26*, 1865-1874.
974 10.1007/s13361-015-1179-x.

975 51. Eng, J.K., Jahan, T.A., and Hoopmann, M.R. (2013). Comet: an open-source MS/MS sequence
976 database search tool. Proteomics *13*, 22-24. 10.1002/pmic.201200439.

977 52. Rad, R., Li, J., Mintseris, J., O'Connell, J., Gygi, S.P., and Schweppe, D.K. (2021). Improved
978 Monoisotopic Mass Estimation for Deeper Proteome Coverage. J Proteome Res *20*, 591-598.
979 10.1021/acs.jproteome.0c00563.

980 53. Elias, J.E., and Gygi, S.P. (2007). Target-decoy search strategy for increased confidence in large-
981 scale protein identifications by mass spectrometry. Nat Methods *4*, 207-214. 10.1038/nmeth1019.

982 54. Huttlin, E.L., Jedrychowski, M.P., Elias, J.E., Goswami, T., Rad, R., Beausoleil, S.A., Villen, J.,
983 Haas, W., Sowa, M.E., and Gygi, S.P. (2010). A tissue-specific atlas of mouse protein
984 phosphorylation and expression. Cell *143*, 1174-1189. 10.1016/j.cell.2010.12.001.

985 55. Savitski, M.M., Wilhelm, M., Hahne, H., Kuster, B., and Bantscheff, M. (2015). A Scalable Approach
986 for Protein False Discovery Rate Estimation in Large Proteomic Data Sets. Mol Cell Proteomics
987 *14*, 2394-2404. 10.1074/mcp.M114.046995.

988 56. Beausoleil, S.A., Villen, J., Gerber, S.A., Rush, J., and Gygi, S.P. (2006). A probability-based
989 approach for high-throughput protein phosphorylation analysis and site localization. Nat Biotechnol
990 *24*, 1285-1292. 10.1038/nbt1240.

991 57. Tyanova, S., Temu, T., Sinitcyn, P., Carlson, A., Hein, M.Y., Geiger, T., Mann, M., and Cox, J.
992 (2016). The Perseus computational platform for comprehensive analysis of (prote)omics data. Nat
993 Methods *13*, 731-740. 10.1038/nmeth.3901.

994 58. Itzhak, D.N., Tyanova, S., Cox, J., and Borner, G.H. (2016). Global, quantitative and dynamic
995 mapping of protein subcellular localization. Elife *5*. 10.7554/eLife.16950.

996